Graduate School Form 30
Updated 1/15/2015

PURDUE UNIVERSITY
GRADUATE SCHOOL
Thesis/Dissertation Acceptance

This is to certify that the thesis/dissertation prepared

By Fan Yang

Entitled

STUDY OF CATALYSTS WITH HIGH STABILITY FOR PROTON EXCHANGE MEMBRANE FUEL CELLS

For the degree of Master of Science in Mechanical Engineering

Is approved by the final examining committee:

Jian Xie
Chair

Yongzhu Fu

Jing Zhang

To the best of my knowledge and as understood by the student in the Thesis/Dissertation Agreement, Publication Delay, and Certification Disclaimer (Graduate School Form 32), this thesis/dissertation adheres to the provisions of Purdue University's "Policy of Integrity in Research" and the use of copyright material.

Approved by Major Professor(s): Jian Xie

Approved by: Jie Chen 7/24/2015

Head of the Departmental Graduate Program Date

STUDY OF CATALYSTS WITH HIGH STABILITY FOR PROTON EXCHANGE MEMBRANE FUEL CELLS

A Thesis

Submitted to the Faculty

of

Purdue University

by

Fan Yang

In Partial Fulfillment of the

Requirements for the Degree

of

Master of Science in Mechanical Engineering

August 2015

Purdue University

Indianapolis, Indiana

This thesis is dedicated to my dear parents for their unconditional love and fully support for my study and research which lead me the path to success. You gave me strength when I was down and helped me to step out of the toughness time. Without you, it is impossible for me to finish my masters degree at IUPUI.

ACKNOWLEDGMENTS

First of all, I will thank my advisor Dr. Jian Xie who helped me on the experiment design for my thesis. He was a brilliant researcher who provided me lots of good ideas that helped me to open my mind. He also helped me to get used to the graduate school life and supported me to continue my graduate study in financial aspect.

I would also like to thank Dr. Qi Liu, Dr. Chuankun Jia, Dr. Zhefei Li, Dr. Le Xin and Dr. Yadong Liu to help me help me a lot on my experiment. They trained me to use the equipment in the lab and taught a lot of background knowledge about both battery and fuel cell. My graduate life will never be so easy without them.

TABLE OF CONTENTS

LIST OF TABLES

LIST OF FIGURES

ABSTRACT

Yang, Fan. M.S.M.E., Purdue University, August 2015. Study of Catalysts with High Stability for Proton Exchange Membrane Fuel Cells. Major Professor: Jian Xie.

The innovation and investigation of catalysts in proton exchange membrane fuel cells are included in this thesis.

In the first part of this work, stability of the catalyst support of PEMFC catalyst is investigated. Nanoscale platinum particles were loaded on two different kinds of carbon supports, nano graphene sheets and functionalized carbon black/graphene hybrid were developed by the liquid phase reaction. The crystal structure of two kinds of catalysts was characterized by X-ray diffractometer (XRD). The morphology and particle size were characterized by scanning electron microscope (SEM) and transmission electron microscope (TEM). Pt loading was measured by thermal gravimetric analysis (TGA). The Brunauer, Emmett and Teller (BET) method was applied to test the surface area of the catalysts. The electrochemical surface area (ECSA) and mass activity during oxygen reduction reaction (ORR) process for two kinds of catalyst were tested by cyclic voltammetry method under different conditions. The stability of the catalysts were tested by accelerated durability test (ADT). The results show that although the mass activity of Pt/graphene is much lower, the stability of it is much better than that of the commercial catalyst. After adding functionalized carbon black (FCB) as spacer, the stability of the catalyst is preserved and at the meantime, the mass activity becomes higher than 20% Pt/XC72 catalyst. The lower mass activity of both catalysts are due to the limitation of the electrolyte diffusion into the carbon support because of the aggregation nature of graphene nano-sheets. After introducing functional carbon black as spacer, the mass activity and ECSA increased dramatically which proved that FCB can be applied to prevent the restacking

of graphene and hence solved the diffusion problem. In the meantime, the durability was still keeping the same as Pt/graphene catalyst.

In the second part of the work, the restacking problem was solved by introducing FCB as spacers between functionalized graphene nanosheets. The same measurement was applied to test the electrochemical performance of Pt/FCB/FG catalyst. The new catalyst showed a higher mass activity compared to Pt/graphene catalyst which meant the restacking problem was partially solved. The durability of the Pt/FCB/FG catalyst was still excellent.

1. INTRODUCTION

The demand for non-renewable fossil fuels such as gas, oil and coal has been increasing significantly after the industrial revolution, which caused more and more serious pollution problems. Those problems have led people to convert to other sources of renewable energy from traditional fuels [1–9]. Fuel cells and batteries are two types of solution with different design concepts that have come to our daily life to replace the traditional fuels in the automotive field [10, 11].

Although the concept of fuel cells came up in the year 1838 which was about 180 years ago, the first commercialized electric vehicles powered by fuel cells were still prototypes until was put into market by the end of this year by Toyota. The bottleneck which hinders the widespread use of fuel cell is its catalyst. The catalyst is made of two major parts, platinum and carbon support. The high cost of Pt and durability of carbon support are two major factors which prevent the commercialization of fuel cells. To figure out these problems, people were trying to decrease the Pt loading while keeping high catalyst activity and enhance the durability of the catalyst by seeking for highly stable carbon support. The durability of proton exchange membrane fuel cells (PEMFCs) is essential for their use as the propulsion system in fuel cell vehicles. The performance loss of the PEMFCs during long-term operation under steady and dynamic conditions has been attributed to the degradation of Pt and Pt alloy catalyst nanoparticles [12–14], the corrosion of carbon supports, and the degradation of the Nafion ionomer network inside the catalyst layer and the Nafion membrane [15–22].

During long term durability tests, one of the major failure causes for the catalysts is the corrosion of the catalyst supports [23]. Currently, carbon blacks (CBs) have been widely used as the supports for Pt and Pt alloy nanoparticle catalysts in PEMFCs [24–26]. However, CB is prone to oxidization as the cell potential rises over 0.8V [27, 28]. The corrosion process of CB will cause the agglomeration of the Pt

nanoparticles and the detachment of the Pt nanoparticles from the supports, resulting in a significant decrease in the ECSA and activity of the catalysts [29] during the course of testing. Moreover, the application of CB in commercialized PEMFCs is restricted because of its low surface area and the fact that some of the Pt nanoparticles are trapped within the pores, which influences the 3-phase reaction [30]. Thus, it is crucial to develop catalyst supports with high carbon corrosion resistance and a high surface area.

In our previous work, we have demonstrated that the higher the degree of graphitization of the carbon support is, the stronger the carbon corrosion resistance is [31,32]. In order to improve corrosion resistance, carbon supports with more graphitic components have been explored [33], such as graphite carbon nanofibers [34], carbon nanotubes [35], ordered uniform porous carbon networks [36], nanographite [37], and reduced graphene oxide (graphene) [38]. These carbon materials have been shown to be more corrosion-resistant than carbon blacks; however, the cost of manufacturing is still a concern. Among all these carbon materials, graphene sheets [39–42] have been investigated extensively due to their high thermal and electrical conductivity, extremely large surface area, and excellent chemical stabilities [38]. Graphene is a highly graphitic sp2 structured two dimensional monolayer of carbon atoms [43]. Recently, graphene has received increased attention as a catalyst support for fuel cell applications [44–46]. Si, et al. [47] synthesized the Pt catalyst supported on a graphene composite by separating the graphene with Pt nanoparticles. However, the long-term durability failure mechanism has yet to be investigated. Graphene oxide (GO) is the oxide form of the graphene sheet and has abundant functional groups (i.e. carboxyl, carbonyl, epoxide, hydroxyl, etc.) [48,49] on both sides of the sheet. Some hydrophilic functional groups will remain on the sheet after the partial reduction of the GO [50]. The presence of such functional groups can provide many anchoring sites for Pt complex ions to form ion clusters/nanoparticles over the surface of the graphene sheets, consequently, promoting the formation of uniformly distributed Pt nanoparticles over the graphene sheet. On the other hand, after the partial GO reduction, the remain-

ing functional groups increase the hydrophilicity of the graphene surface, leading to improved dispersion of the Pt nanoparticles supported on graphene sheets in aqueous media. Improved dispersion is essential for developing a high-performance membrane electrode assembly (MEA). Here we report a rapid, simple, one-step synthesis procedure to fabricate the graphene-supported Pt nanoparticle catalyst (Pt/graphene) in an aqueous EG solution for PEMFC application. Also, we demonstrate the mechanism of the catalyst failure and compare durability between the 20% Pt/XC72 and our own Pt/graphene catalyst. The commercialized catalyst was made by platinum and amorphous carbon black as carbon support which was prone to corrosion. Here, we used nanosheets of graphene which was a highly graphitic structure and had a very high stability toward corrosion during cycling process. However, sp2 hybridization makes graphene sheets to tend to aggregate together which causes diffusion problem. We then proposed a new method to deal with the diffusion problem by applying functionalized carbon black as spacer to prevent the restacking of graphene nanosheets. Bonded on the surface of graphene nanosheets by strong electrostatic force.

2. BACKGROUND

2.1 Proton Exchange Membrane Fuel Cell

2.1.1 Fuel Cell

With the increasing demand for energy after the Industrial Revolution, the fossil fuel consumption speed has been much faster than its regeneration rate, which has caused the increasing price and shortage of fossil fuel in recent years. In the meantime, pollution from industry and automobiles is also another big issue. To settle these problems, high efficiency and clean renewable energy conversion devices need to be developed. Due to the Carnot efficiency limit, current heat engines are not effective enough to save fossil fuel energy. Fuel cells are good candidates for the next generation energy conversion devices because of their high efficiency. Also, the products of fuel are water and carbon dioxide, which make fuel cells absolute clean energy conversion devices compared to Carnot engines.

Fuel cells are divided into six major types [51]:

(1) Proton exchange membrane fuel cells (PEMFC)

(2) Direct methanol fuel cells (DMFC)

(3) Alkaline fuel cells (AFC)

(4) Molten carbonate fuel cell (MCFC)

(5) Solid-oxide fuel cell (SOFC)

(6) Phosphoric acid fuel cells (PAFC)

The operation parameter and performance of different kinds of fuel cells are listed in Table 2.1 [51].

Although fuel cells have lots of advantages, there are several major challenges that have to be settled. Cost is the biggest barrier that prevents the fuel cells from commercialization.

Table 2.1. Characteristics of different kinds of fuel cells [51]

	PEMFC	DMFC	AFC	PAFC	MCFC	SOFC
Primary application	Automotive and stationary power	Portable power	Space vehicles	Stationary power	Stationary power	Vehicle aux power
Electrolyte	Polymer membrane	Polymer membrane	30-50% KOH in H_2O	100% H_3PO_4	Molten carbonate	YSZ
Operating temperature	50 - 100 °C	0 - 60 °C	50 - 200 °C	155 - 220 °C	600 - 700 °C	700 - 1000 °C
Charge carrier	H^+	H^+	OH^-	H^+	CO_3^{2-}	O^{2-}
Catalyst	Pt	Pt/Ru	Pt	Pt	Ni	Perovskite
Fuel	H_2	Methanol	H_2	H_2	H_2, CO_2, CH_4	H_2, CO
Power density (kW/m^3)	3.8-6.5	0.6	1	0.8-1.9	1.5-2.6	0.1-1.5
Efficiency	50-60%	30-40%	50-60%	55%	55-65%	55-65%

2.1.2 Proton Exchange Membrane Fuel Cell (PEMFC)

Proton exchange membrane fuel cells which are also known as polymer electrolyte fuel cells are the most popular type of fuel cells in recent research and will be applied in the next generation electric vehicles. There are three major components of PEMFC which are shown in Fig. 2.1. Flow field is used to transport oxygen and hydrogen gas in cathode and anode sides and also transport electrons to loading. Flow field is made of high purity graphite which has a very high conductivity. Gas diffusion layer (GDL) is used as electrode backing to uniformly distribute the gas in PEMFC [52]. Most of GDLs are made of carbon cloth or carbon fiber paper which guarantees the high electron conductivity [53]. Membrane electrode assembly, which is the most important part in PEMFC, is used to carry the catalysts and ionomer. The performance of MEA

directly influences the performance of the whole cell. The structure and function of MEA will be discussed in Section 2.1.3.

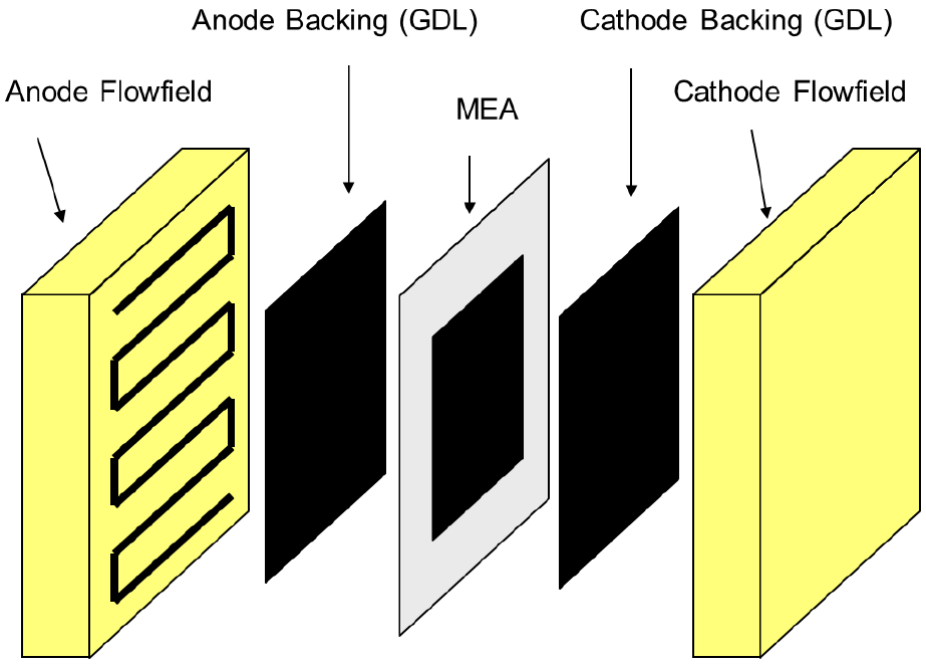

Figure 2.1. Components of PEMFC

The schematic for the operation of PEMFC is shown in Fig. 2.2. The anode reaction is shown in Equation 2.1. In the anode side, hydrogen was oxidized to protons which travel across the Nafion membrane to the cathode side.

$$2H_2 \rightarrow 4H^+ + 4e^- \tag{2.1}$$

In the cathode side, the reaction is shown in Equation 2.2. The oxygen gas is reduced and bonded with protons to form H_2O molecules.

$$O_2 + 4H^+ + 4e^- \rightarrow 2H_2O \tag{2.2}$$

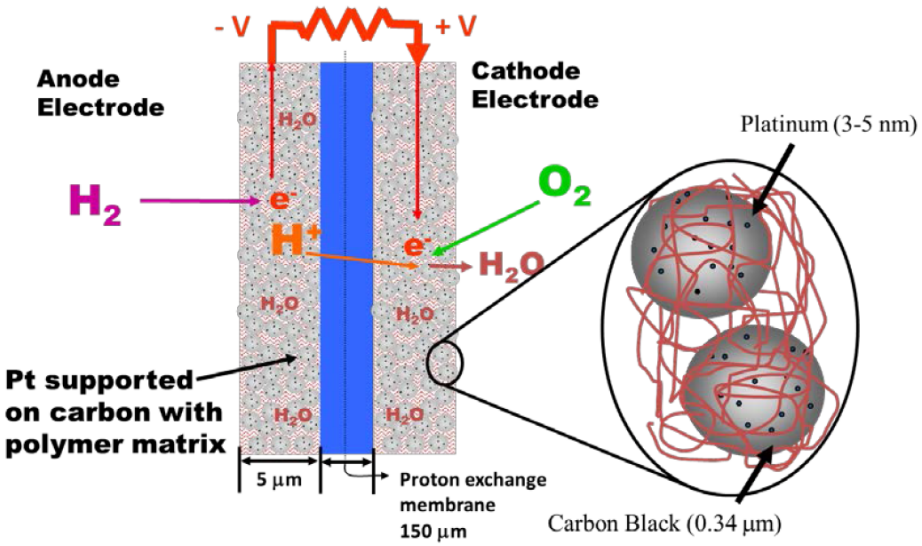

Figure 2.2. Schematic for operation of PEMFC

2.1.3 Membrane Electrode Assembly (MEA)

MEA is the core part of PEMFC. There are two major components of MEA.

The Nafion membrane is used to transport protons from the anode side to the cathode side. Nafion is the commercial name for a series of fluorinated sulfonic acid copolymers developed by DuPont's company which is shown in Fig. 2.3. It is a polymer which chain is ending with the sulfonic group [54]. It has been proved that protons are transferred through Nafion membranes by the vehicle mechanism [55]. The sulfonic group helps the transport of protons. The ionic conductivity of the Nafion membrane is about 0.2 S/cm which is much higher than other products.

The second part of MEA is the catalyst layer. Platinum is used as the catalyst in PEMFC because it has the highest catalytic activity. The application of pure Pt in PEMFC catalyst is impossible since the price for such noble metal is so high. People then tried to find a composite catalyst that can achieve relative high catalytic activity. Carbon black was then found to be a good candidate to be used together with Pt as catalyst instead of pure Pt. Although carbon is pretty compatible with

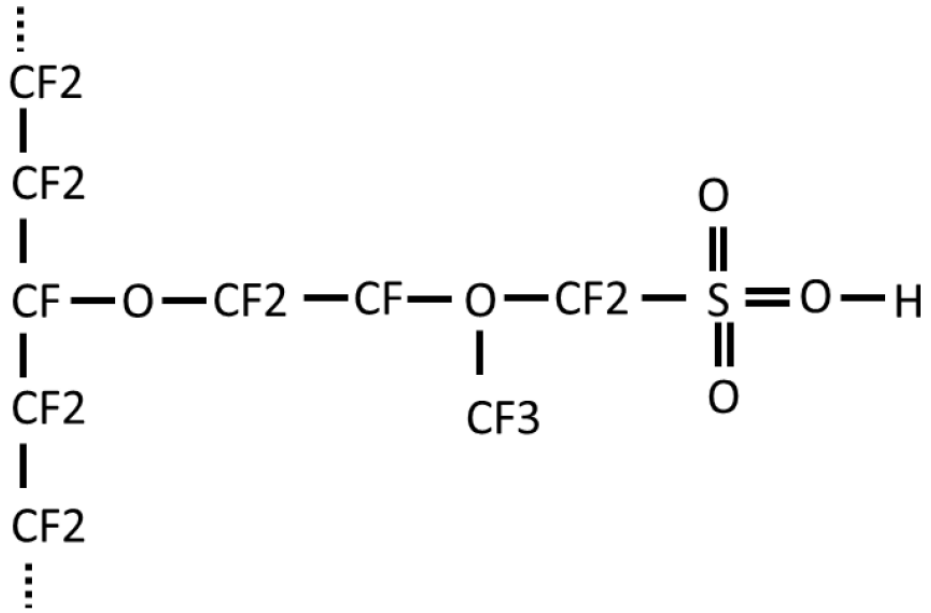

Figure 2.3. Structure of Nafion

Pt, its durability is poor during cycling [23]. The amorphous nature of carbon makes it prone to corrosion; thus a new highly stable catalyst support needs to be found.

2.2 Graphene

Graphene which is made of single layer sp2 hybridized carbon atoms is famous for its extraordinary electron conductivity. The structure of graphene is shown in Fig. 2.4.

Graphene is a 2-D material which is made of a single layer of carbon atoms. Each carbon atom is bonded to 3 carbon atoms by covalent bonds. The forth valence electron of the carbon atom forms a π bond with the other 5 atoms in the same ring. Due to the π bond on the whole surface of graphene, the electron conductivity is very high because the electrons can flow freely along the graphene plane. This structure makes all valence electrons in carbon atoms saturated and thus makes the graphene a very stable structure. According to our previous research [37], the material with higher graphitic degree has a higher corrosion resistance. Since the graphene is a single

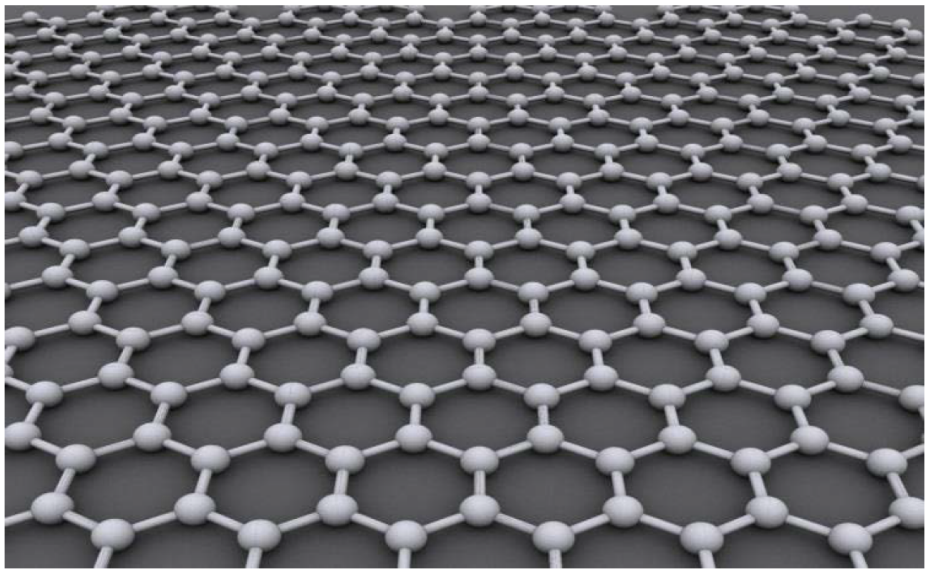

Figure 2.4. Structure of graphene [56]

layer of graphite, it is the material with the highest graphitic degree which makes it to be a highly corrosion resistive material. With less carbon corrosion in the catalyst layer, Pt nano particles will be better embedded on the surface of the carbon support without much detaching and aggregating to keep better catalytic performance. The single layer of carbon atoms is not thermodynamically stable and tends to aggregate to the structure of more layers. The graphene nanosheets can be synthesized from the reduction of graphene oxide according to Hummer's method [57, 58]. Graphene oxide (GO) is the oxidized form of graphene which can be obtained by the oxidation of natural graphite. There are lots of defects and oxygen containing function groups on the surface of GO (Fig. 2.5) which facilitate the better dispersion into water. After being reduced to graphene, part of the oxygen containing groups will still be remaining on the surface of graphene, such as hydroxyl, epoxy and ketone. Such function groups will help graphene to better disperse into water to reduce the restacking of graphene.

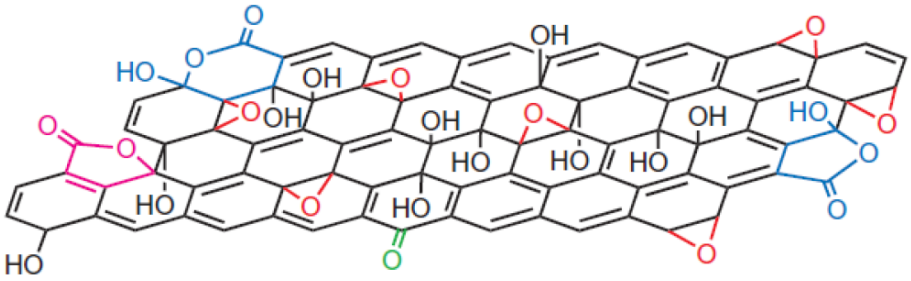

Figure 2.5. Structure of graphene nanosheets prepared by reduction of graphene oxide [59] Adapted by permission from Macmillan Publishers Ltd: [Nature Chem] (vol. 1, pp. 403-409), copyright (2009).

3. IMPROVEMENT OF CARBON SUPPORT FOR FUEL CATALYSTS

3.1 Experimental

3.1.1 Experiment Materials and Instruments

Materials

All materials used are listed in Table 3.1.

Table 3.1. Materials

Chemical name	Purity	Provider
Chloroplatinic acid ($H_2PtCl_6xH_2O$)	99.9%	Acros Organics
Carbon black Vulcan XC-72	Not specified	Cabot, MA
Nafion solution	5wt%	Ion Power Inc.
Graphite powder	99.8%	Alfa Aesar
Ethylene glycol	99.8%	Sigma-Aldrich
Sodium borohydride ($NaBH_4$)	99%	Acros Organics
Ammonium hudroxide	28-30wt%	Fisher Scientific
70% perchloric acid solution	99.999%	Fisher Scientific
Isopropanol alcohol (IPA)	99.9%	Fisher Scientific
High purity de-ionized (DI) water	18MΩ	Millipore
20% Pt/XC72 catalyst (E-TEK)	Not specified	BASF
Hydrogen (H_2)	5.0 UHP	Praxair
Oxygen (O_2)	5.0 UHP	Praxair

All chemicals were used as received.

Instruments

All instruments used are listed in Table 3.2.

Table 3.2. Instruments

Instrument	Provider
Electrochemical workstation	Bio-Logic, TN, USA
Ag/AgCl reference electrode	Pine instruments, PA, USA
Electrode rotator	Pine instruments, PA, USA
Rotating disk electrode (RDE)	Pine instruments, PA, USA
X-Ray diffractometer	Siemens
Thermogravimetric analyzer (TGA)	TA instrument
Transmission electron microscopy	From Argonne National Lab
Gas sorption analyzer	Quantachrome Instruments, FL, USA
Freeze drier	Labconco, MO, USA
Vacuum oven	VWR
Centrifuge	Thermo scientific
Ultrasonic bath	Branson, CT, USA

3.1.2 Experiment Methods

Synthesis of Graphene Oxide

Graphene oxide was prepared by a modified Hummer's method [57, 60]. Ten grams of graphite flakes were mixed with 50ml concentrated H_2SO_4, 10g $K_2S_2O_8$ and 10g P_2O_5. The mixture was then heated to 80°C and then cooled down to room temperature under constant stirring. The mixture was then filtered and washed with DI water. The remaining product was dried in a vacuum oven at 80°C.

After the pre-oxidation process, 2g of pre-oxidized graphite and 1g of $NaNO_3$ was mixed with 46 ml of concentrated sulfuric acid in a 500ml round-bottom flask. After stirring for 30 min, 6g $KMnO_4$ was added into the mixture above and the round-bottom flask was transfered to an ice bath to be cooled down. Then 92 ml DI water was added into the mixture dropwise. The mixing of DI water and H_2SO_4 increased the temperature to 95-100°C and the solution was stirred for 15 min followed by adding 280 ml water for dilution and 10 ml H_2O_2 for further oxidation. The solution

was then centrifuged and washed by water. After the last centrifuge, the remaining solid was dispersed uniformly into water and was ready to be used.

Synthesis of Pt/graphene Catalyst

80 mg GO was dispersed into 40 mL DI water by ultrasonic stirring for at least 30 min, followed by the addition of 5 mL IPA and 10 mL EG. The resulting mixture was continuously stirred overnight. Afterwards, 2 mL platinum precursor [$H_2PtCl_6.xH_2O$] salt solution (10 mgPt/mL) was added drop wise into the solution under mild stirring, and further stirred for 2 h. Then, 15 mL freshly prepared $NaBH_4$ solution (2 mg /mL) was drop-wise added into the mixture solution [33]. The mixture was heated for 5 h at 95°C under stirring. Then 4 mL ammonium hydroxide was added into the mixture to adjust the pH to 11. The resulted solution was cooled to room temperature. Finally, the products were collected by repeated filtration and washed with DI water and ethanol, and dried in a freeze dryer.

3.1.3 Characterization

The phase compositions of the synthesized catalysts were characterized by X-ray diffractometer (XRD). By comparing the characterization diffraction peaks, we can identify the phase in the sample. By applying Bragg's equation, we can calculate the d-space of the crystal structure and by applying Scheerer's equation, we can get the particle size.

The morphology, particle size and size distribution of the catalysts powders were examined using TEM. The graphene nanosheets and Pt particles can be seen clearly under high magnification. The particle size distribution can be counted statistically by using the software "ImageJ".

Thermogravimetric analysis (TGA) was carried out to determine the Pt loading on the graphene. The sample in the crucible was heated to certain temperature and the weight of the sample was recorded at real-time.

Gas sorption analyzer was applied to measure the specific surface area. The Brunauer, Emmett and Teller method was used to measure the surface area by recording the N_2 absorption on the surface of the sample.

Pore distribution of the Pt/graphene catalyst was measured using a mercury porosimetry analyzer. The sample chamber was first turned into a vacuum and then the mercury was pushed into the chamber. The pressure was added into the chamber by a compressor from 0 to 60000 psi and the intrusion volume of mercury was recorded. By building the model according to Washburn's equation [61], the differential of specific v with respect to the radius r of the pores in the Washburn's model was calculated. By plotting dv/dr vs. r, we can get the pore size distribution of our sample.

3.1.4 Electrochemical Measurements

The synthesized catalysts were characterized using a rotating disc electrode (RDE) for their electrochemical performance. A catalyst ink was prepared by adding the calculated amount of both catalyst powder and 5wt% Nafion solution into 2 ml IPA aqueous solution (IPA: H_2O = 1:4, volumetric ratio) under sonication until a uniformly dispersed catalyst ink was formed. Then, the calculated volume of ink was dropped onto the surface of a mirror-polished RDE which surface area was 0.196 cm^2. The RDE was then rotating at the speed of 600 rpm until the ink was fully dried. The Pt loading on the RDE was 17.3 ug/cm^2 for all catalyst samples and the Nafion content is 20wt% for all catalysts in the thin film on the RDE.

All electrochemical measurements were carried out on a Bio-Logic VSP electrochemical workstation (Bio-Logic USA, Knoxville, TN) with a standard three-electrode system at room temperature. An Ag/AgCl double junction reference electrode (RREF0024, Pine Research Instrumentation) was used as reference electrode, a Pt foil was used as counter electrode and the catalyst coated thin film RDE was used as the working electrode. Nitrogen gas was purged into 0.1 M $HClO_4$ electrolyte

for at least 30 min first. Then, the working electrode was first electrochemically cleaned by potential cycling between 0.00 and 1.20 V at 1000 mV/s for 300 cycles. After the cleaning, cyclic voltammetry (CV) measurements were performed at a scan rate of 20 mV s-1 between 0.05 and 1.00 V (vs. SHE) in nitrogen saturated $HClO_4$ electrolyte. The electrochemical surface area (ECSA) was calculated by integrating hydrogen adsorption charge.

Oxygen reduction reaction (ORR) in O_2 saturated 0.1 M $HClO_4$ electrolyte was recorded on the rotating disk electrode which was rotating at the speed of 1600 rpm at room temperature. The scan rate was 20 mV s-1 and the voltage range was 0.20 V- 1.10 V. The double layer background was measured in the N_2 saturated 0.1 M $HClO_4$ electrolyte under the same scan as ORR test.

The accelerated durability test (ADT) was carried out to reveal the stability of the catalysts. Potential was swept from 0.60 V to 1.20 V with saturated nitrogen at the scan rate of 20 mVs^{-1}. CV was tested every 200 cycles and ORR was tested before and after ADT.

3.2 Result and Discussion

3.2.1 Characterization of Pt/graphene Catalyst

The TGA results of pure GO, Pt/graphene is shown in Fig. 3.1. Pure GO showed two major weight loss steps. The first step with a weight loss of about 25% occurred in the temperature range of 100 °C to 300 °C, which resulted from the removal of oxygen-containing functional groups. The weight loss in the second step occurring between 500 °C and 600 °C, was about 40wt%, which might correspond to the further thermal decomposition of oxygen-containing functional groups and graphene. There was no rapid weight loss in the range of 100 °C - 300 °C for Pt/graphene indicates that most of the oxygen-containing groups was removed from the GO sheets during synthesis. The result reveals that the GO and Pt were synchronous reduced. The nal loading of Pt nanoparticles was 37.5wt% in Pt/graphene catalyst.

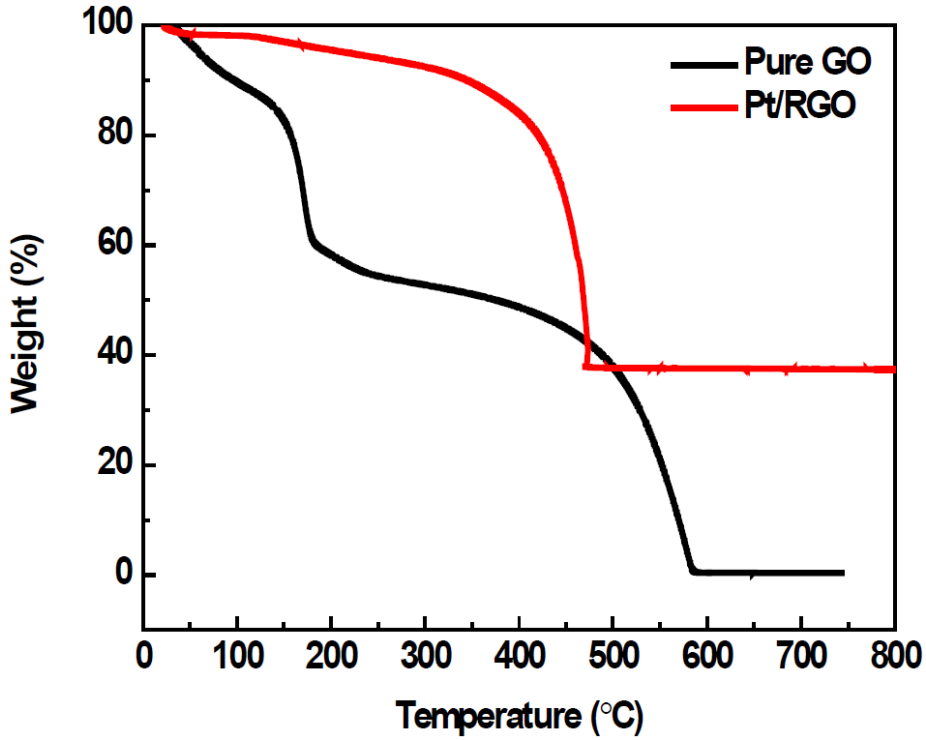

Figure 3.1. TGA curve of Pure GO (black) and Pt/graphene catalyst (red)

The XRD patterns of pure GO and Pt/graphene catalyst are shown in Fig.3.2. The peak of pure GO appeared at around $2\theta = 12.3°$. For Pt/graphene catalyst, the characteristic diffraction peak of GO is shifted to $2\theta = 14.5°$, suggesting that the interlayer spacing is smaller than that of pure GO according to Bragg's law . This may be due to the removal of part of the oxygen-containing functional groups from the surface of pristine GO sheets. These results reveal that part of GO is reduced to graphene. The characteristic diffraction peak of the pure graphene (002) appears at $2\theta = 24.5°$, which is about 3° larger than that in Pt/graphene. The results indicate that the interlayer spacing in Pt/graphene is larger than that of pure graphene. This may be because part of the graphene still have the oxygen-containing functional groups which had not been completely removed during the simultaneous synchronous reduction process [62,63]. Furthermore, the representative diffraction peaks at $2\theta = 39.7°, 46.2°, 67.8° and 81.3°$ observed on the Pt/graphene are matched well to the characteristic (111), (200), (220) and (311) crystalline planes of

Pt, respectively, revealing that Pt precursor ($PtCl_6^{2-}$) was successfully reduced by EG and $NaBH_4$ [64]. The mean particle size of Pt was calculated from XRD patterns by Scheerer's formula based on the the Pt (1 1 1) planes and the average Pt nanoparticle size is determined to be 2.3 nm in diameter.

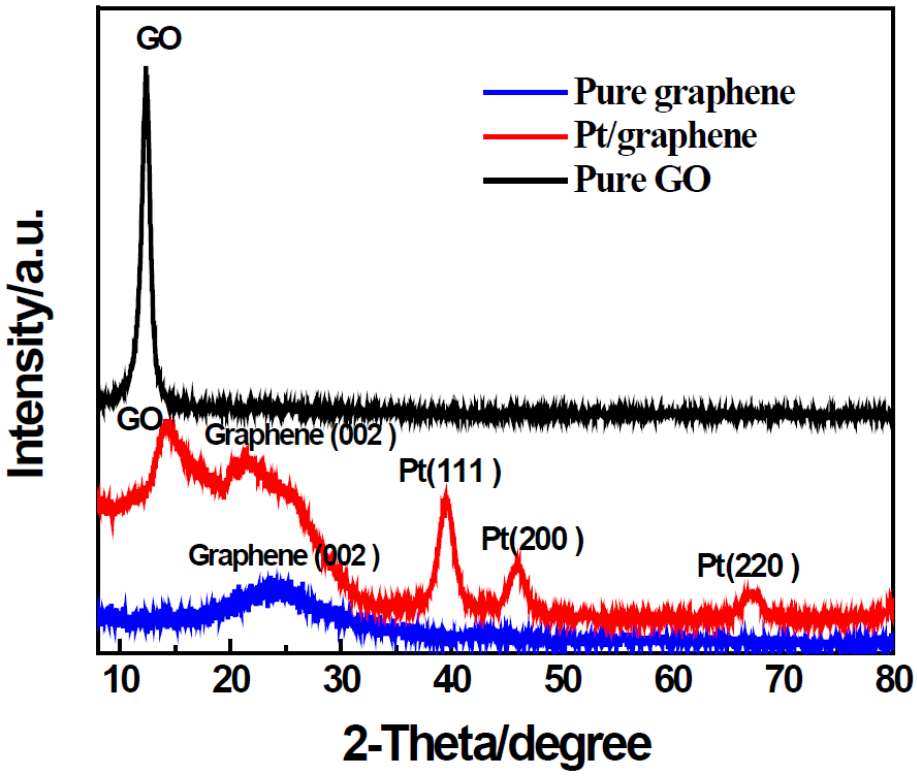

Figure 3.2. XRD pattern of pure GO (black), Pt/graphene (red) catalyst and pure graphene (blue)

TEM images of 20% Pt/XC72 and Pt/graphene catalysts before and after ADT are shown in Fig. 3.3. As can be seen in Fig. 3.3a, Pt particles are distributed isolated on the surface of XC-72 carbon support without much aggregation. However, after ADT (Fig. 3.3b), Pt particles aggregated together and formed much large Pt particles which was caused by the carbon corrosion. During the carbon corrosion process, the carbon was corroded and the contact between carbon and Pt particles was destroyed which caused the migration of Pt nanoparticles. The result for Pt/graphene catalyst was shown in Fig. 3.3c and 3.3d. Although we could still see some aggregation of Pt

nanoparticles, few dissolution was observed. The result confirmed that graphene was a better catalyst support than XC72.

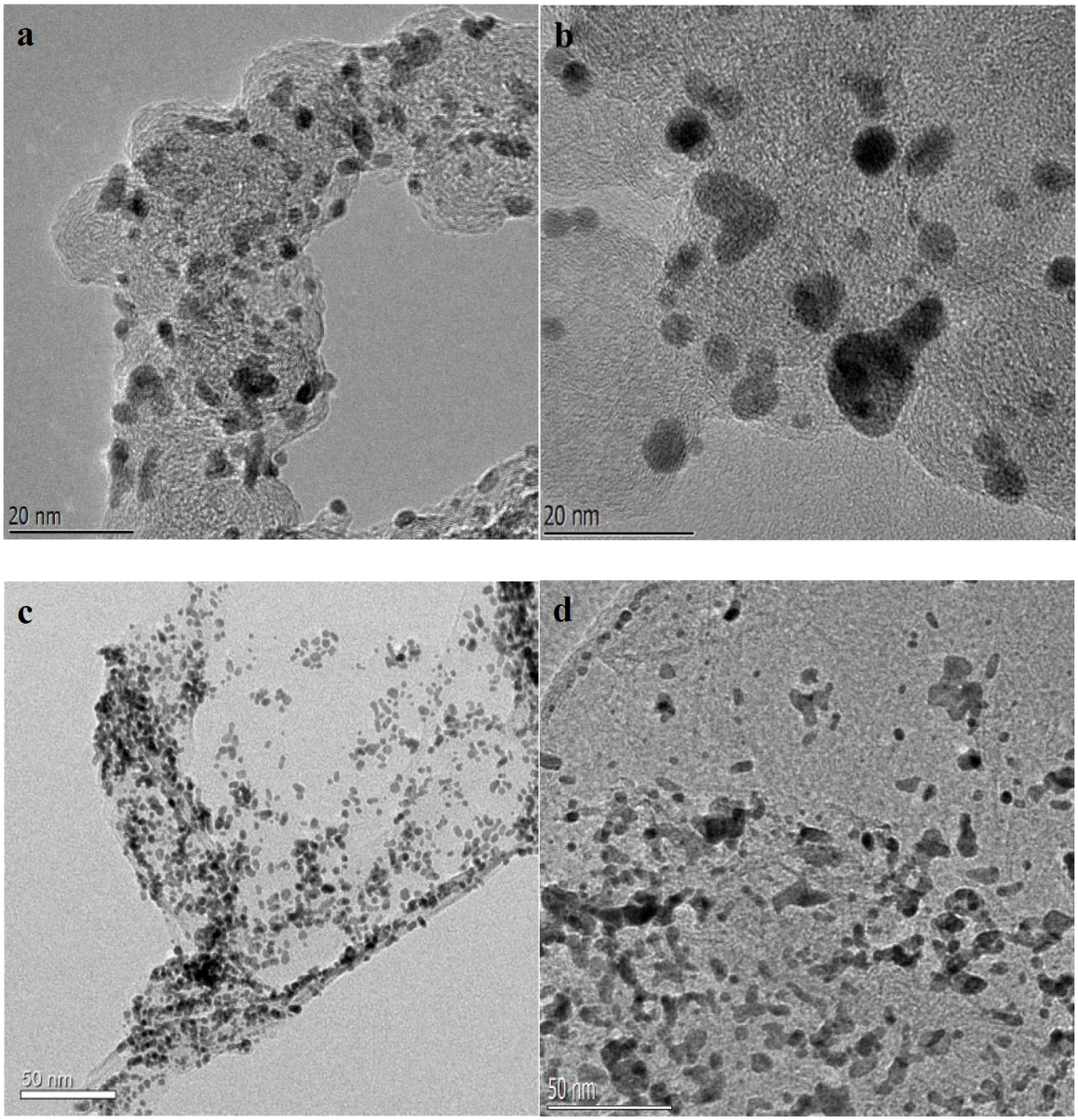

Figure 3.3. TEM picture of (a) 20%Pt/XC72 catalyst before ADT; (b) 20%Pt/XC72 catalyst after ADT; (c) Pt/graphene catalyst before ADT and (d) Pt/ graphene catalyst after ADT

Particle size distribution of 20% Pt/XC72 and Pt/graphene catalyst are shown in Fig. 3.4. The particle size of the Pt in Pt/graphene catalyst distributed within the

range of 0.2-5.1 nm in diameter. and the average particle size of Pt nanoparticles is about 2.65 nm (inset in Fig. 3.4a), which is consistent with the XRD result. The Pt nanoparticles are most in the sphere shape and a few aggregates can be seen (Fig. 3.4b) at a higher magnification. However, the average particle size of Pt in Pt/XC72 catalyst was 3.3nm which is a little larger than that of Pt in Pt/graphene catalyst. After ADT, the size of Pt in Pt/graphene catalyst increased by 56%, however, the diameter of Pt in Pt/XC72 catalyst increased by 76%, which also indicated that corrosion is more serious in Pt/XC72 than Pt/graphene catalyst during ADT.

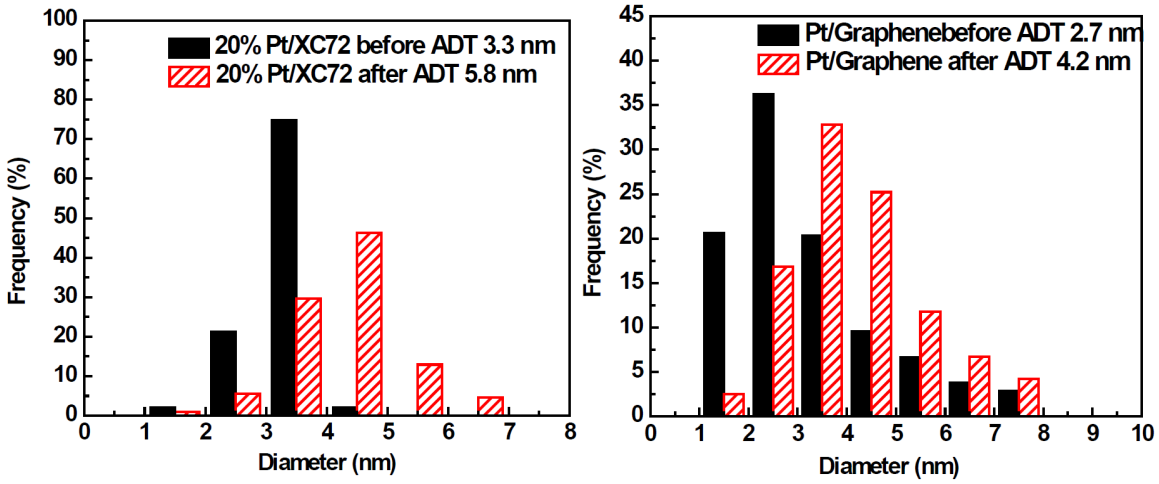

Figure 3.4. Pt particle size distribution of (a) 20% Pt/XC72 and (b) Pt/graphene catalyst

The average surface of graphene nanosheet measured by BET method was $65m^2/g$ which was much lower compared to the theoretical value ($2630m^2/g$). The pore size distribution of Pt/graphene catalyst is shown in Fig. 3.5. It can be seen that most of the pores are 4 nm or even smaller which are around 1 nm. This indicates the restacking of the graphene.

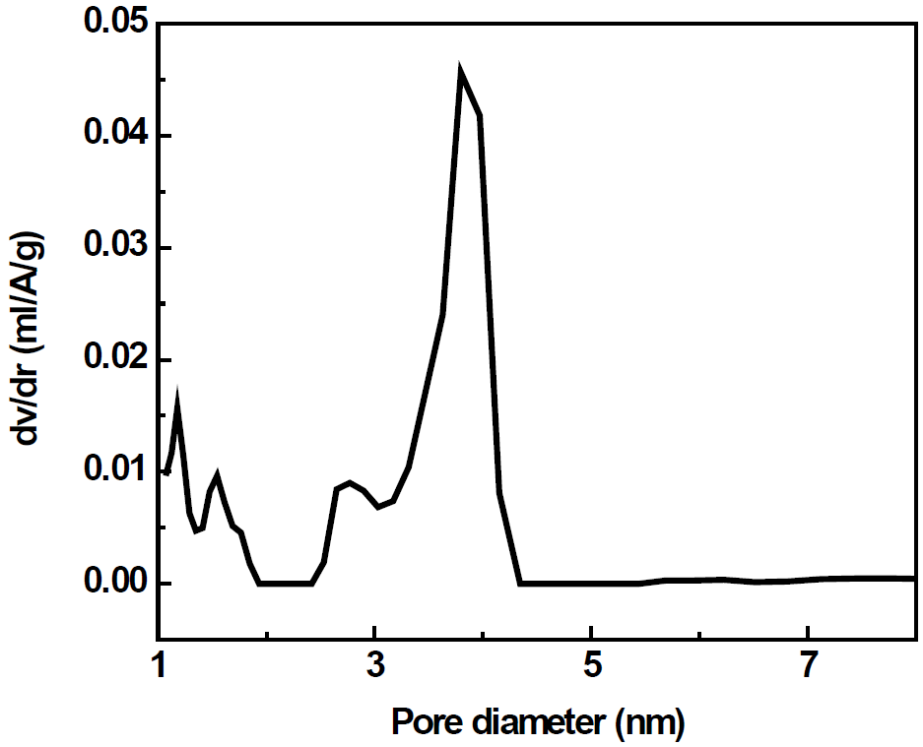

Figure 3.5. Pore size distribution of Pt/graphene catalyst

3.2.2 Electrochemical Performance of Pt/graphene Catalyst

The result of the CV and ORR test of the Pt/graphene catalyst at room temperature are shown in Fig. 3.6. The 20% Pt/XC72 shows clear desorption/adsorption peaks at 0.14 V and 0.22 V which correspond to the [110] and [100] index face of Pt cuba-octhedra particle, respectively. In addition, the Pt/graphene catalyst showed a less double layer charging (Fig. 3.6). The ECSAs of these catalysts are calculated from the integration of the CV curves between 0.05 V to 0.40 V of hydrogen desorption or adsorption charges after double-layer charging correction using the equation in reference [65]. The ECSA value for Pt/graphene is 35.12 m^2/gPt which is much lower than that of the 20% Pt/XC72 (65.05 m^2/gPt), which contradict the size of these two catalysts, 2.65 nm vs. 3.32 nm (Pt/graphene vs. Pt/XC72) [23]. The smaller Pt nanoparticles should result in higher ECSA. It is anticipated that such low ECSA from Pt/graphene catalyst was due to the restacking of graphene nanosheets during

the catalyst synthesis. In spite of the single layered structure of GO in the precursor solution, during the synchronous reduction process, graphene tended to restack to form a multilayer structure, which reduce the sites for Pt nanoparticles to anchor. Another possibility is that the Pt nanoparticles are formed over the graphene sheet first, then, during the reducing process, some of Pt/graphene sheet restack to form multi-layer structure. The gap between neighboring Pt/graphene sheets is so small that the proton transfer is hindered. According to the BET result, the average specific surface area of graphene is 65 m^2/g which is much lower than that of pure graphene. The low specific surface area also confirmed the agglomeration of the 2-D structure graphene which tended to form a 3-D structure. The pore size distribution is centered on 4 nm from BET result which proved that the second hypothesis may be correct. Thus, without appropriate surface area accessible for Pt precursor ions, between layers, the ECSA of Pt/graphene catalyst became lower.

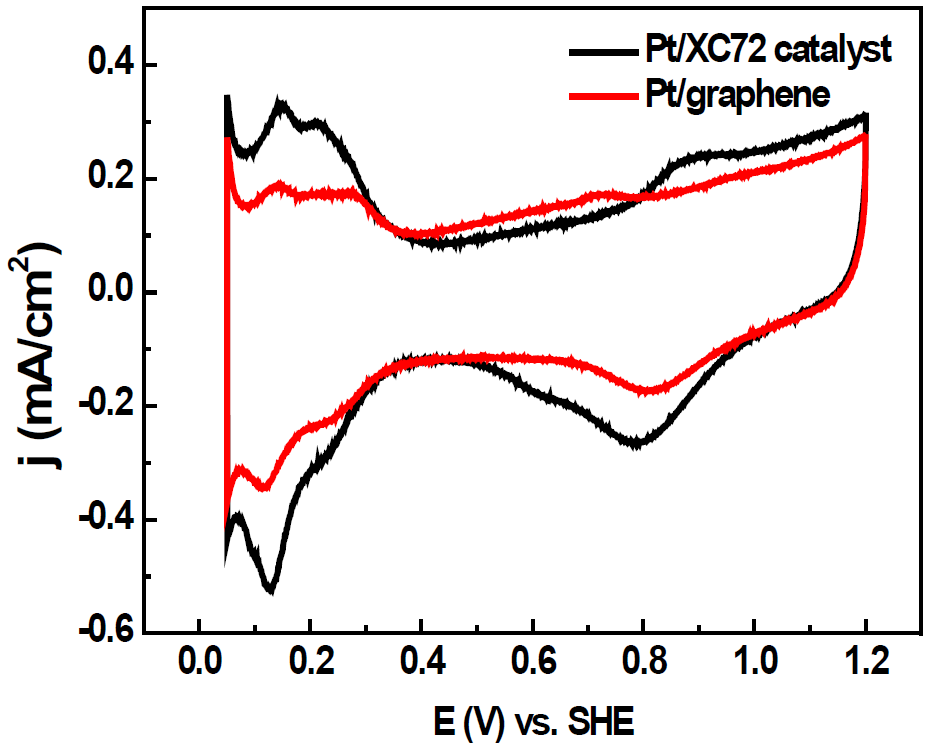

Figure 3.6. CV of Pt/XC72 catalyst and Pt/graphene catalyst

Polarization curves for oxygen reduction reaction (ORR) in O_2 saturated 0.1 M $HClO_4$ electrolyte was carried out on a RDE at the rotating rate of 1600 rpm. It can be seen from Fig. 3.7 that the Pt/graphene has a slightly lower half-wave potential (0.75 V) compared to that of the 20% Pt/XC72 catalyst (0.80 V), suggesting that at the same voltage (0.9 V), the ORR proceeds with much higher rate (30.00 mA/mgPt) at the 20% Pt/XC72 catalyst than that (76.00 mA/mgPt) of Pt/G catalyst. For the Pt/graphene catalyst, the current density in the mixed control region (between 0.50 and 0.85 V) of both kinetic and diffusion is higher than for a 20% Pt/XC72. Meanwhile, the diffusion-limiting current (below 0.5 V) is also higher for 20% Pt/XC72 than that for Pt/graphene. The ORR activity of the catalysts can be calculated with the kinetic current at 0.9 V on RDE calculated using KouteckyLevich equation. As calculated, the Pt mass activity on the Pt/graphene was 30.00 mA mg-1Pt, which was lower than that on the 20% Pt/XC72 (76.00 mA mg-1Pt). The lower mass activity of Pt/graphene catalyst was also due to the restacking of graphene nanosheets which was consistent with the result of the lower ECSA. The restacking leads to a lower surface area of graphene sheet accessible for Pt precursor ions, which result in poor dispersion of Pt nanoparticles over the graphene surface. High mass activity of 20% Pt/XC72 catalysts was attributed to the improved dispersion of Pt nanoparticles over the surface of XC72 because of the higher surface area of XC72 (250 m^2/g) than that of graphene sheets (65 m^2/g). This indicated that the restacking of graphene sheets results in lower surface area for Pt precursor ion access, leading to a relative low RDE ORR performance.

In order to compare the stability of Pt/graphene and 20% Pt/XC72, the accelerated durability tests (ADTs) were also carried out in N2-saturated 0.1 M $HClO_4$ electrolyte at room temperature. The CV curves and the polarization curves of both Pt/graphene and 20% Pt/XC72 at different ATD cycles are shown in Fig. 3.8 and the calculated ECSA retention and mass activity of both catalysts at different ADT cycles are shown in Fig. 3.9. As can be seen in Fig. 3.8a and 3.8b, the hydrogen

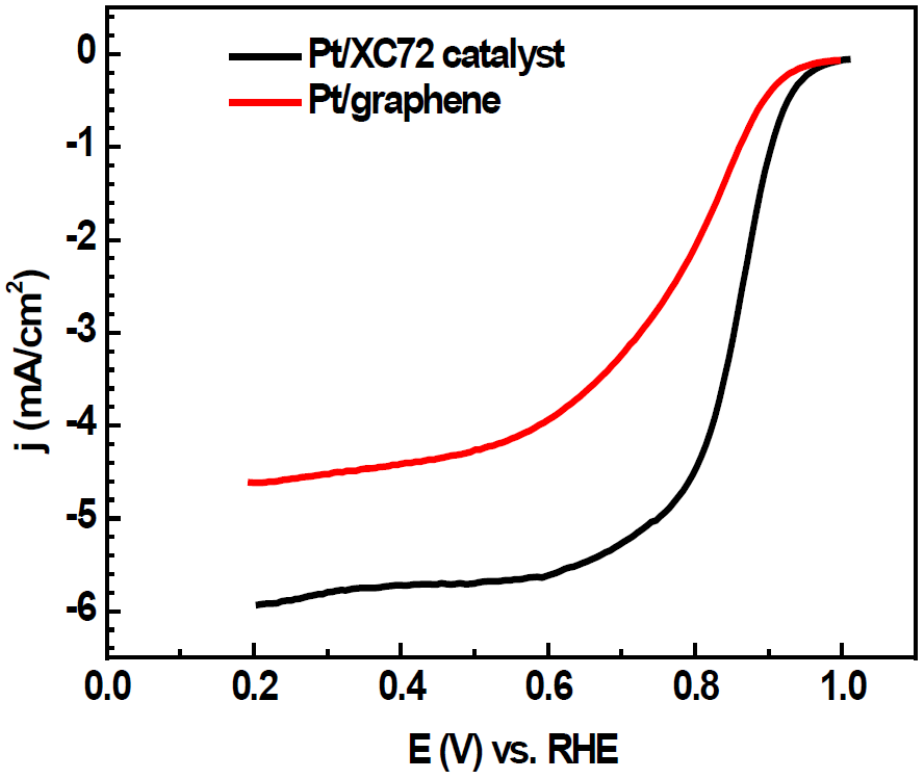

Figure 3.7. Polarization curve of Pt/XC72 and Pt/graphene catalyst

adsorption and desorption peaks both decreased with ADT cycles, which indicated the aggregation of Pt particles and the corrosion carbon support material.

To further compare the stability of Pt/graphene and 20% Pt/XC72 catalysts, the ECSA and mass activity retention during ADTs was shown in Fig. 3.10, table 3.3 and table 3.4. It can be seen that the ECSA of 20% Pt/XC72 keeps dropping and only 55% ECSA left after ADTs while the ECSA of Pt/graphene catalyst still has 66% ECSA left. Meanwhile, the decay rate of ECSA retention of 20% Pt/XC72 is 4.5%/100 cycle while Pt/graphene has two distinct decay rates, first, 11.5%/ 100 cycle before 200 cycles, then 3.4%/100 cycles, after 200 cycle, indicating a much stronger corrosion resistance. The result of the mass activity retention also showed the same trend (Fig. 3.10b). Although the mass activity of both Pt/graphene and 20% Pt/XC72 drop significantly before 200 cycles (24%/100 cycles vs. 30.5%/100 cycles) and slow down afterward (4.0%/100 cycles vs. 3.8%/100 cycles), the Pt/graphene catalyst still keeps

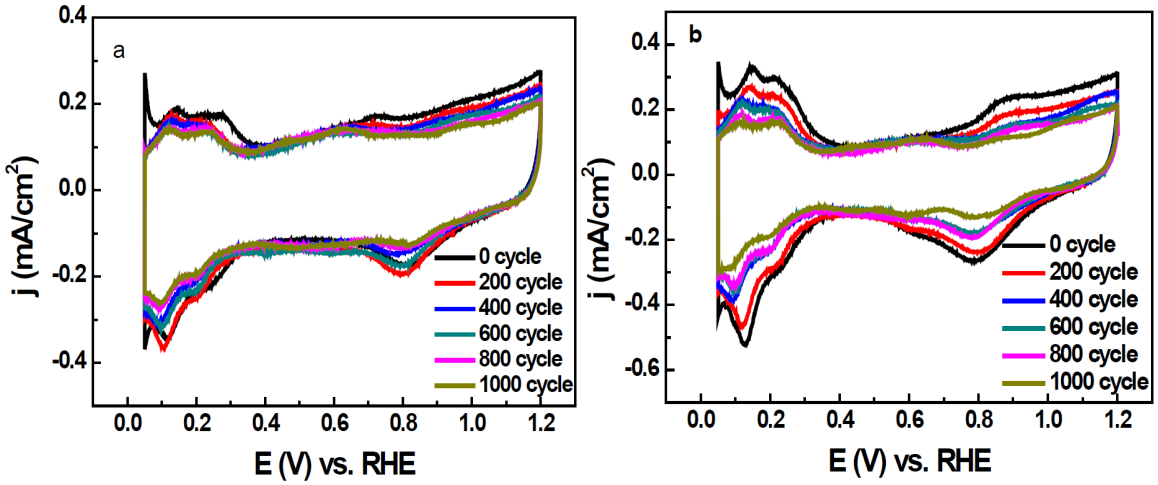

Figure 3.8. CV curve during ADT of (a) Pt/graphene catalyst and (b) Pt/XC72 catalyst

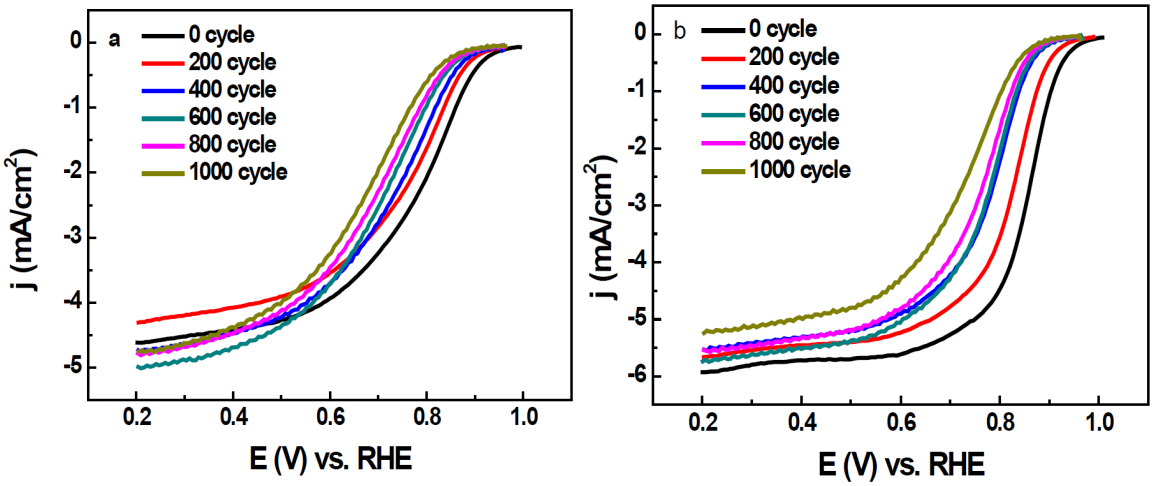

Figure 3.9. Polarization curve during ADT for (a) Pt/graphene catalyst and (b) Pt/XC72 catalyst

20% of the initial mass activity which is much higher than that of 20% Pt/XC72 (9% retention).

In addition to the agglomeration of Pt nanoparticles during ADT cycling, the detachment of Pt nanoparticles from the support was also the cause of ORR performance loss. After the carbon corrosion process, the Pt support with lower corrosion

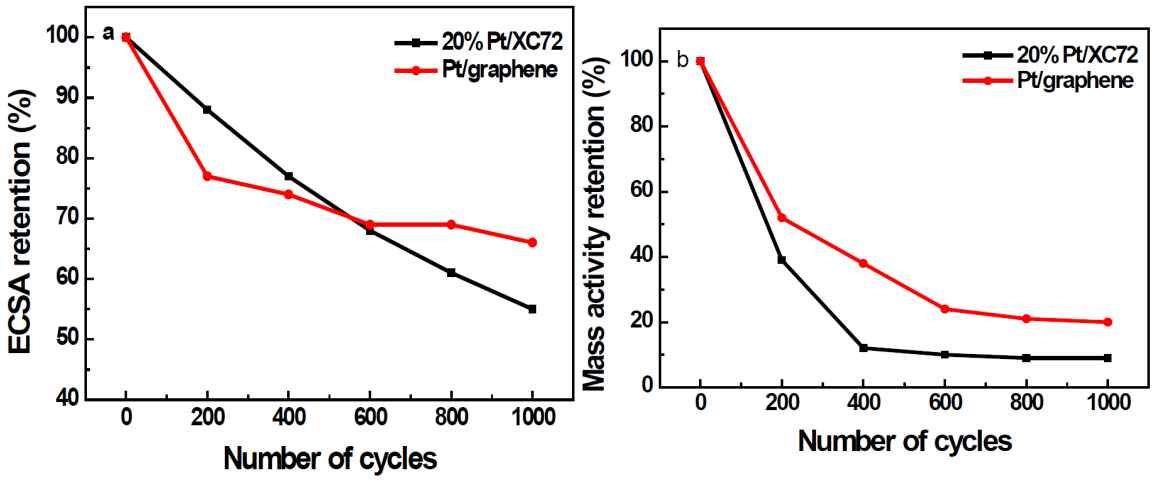

Figure 3.10. (a) ECSA and (b) mass activity retention of Pt/XC72 and Pt/graphene catalyst

Table 3.3. ECSA retention for 20% Pt/XC72 catalyst and Pt/graphene catalyst

	20% Pt/XC72 (%)	Pt/graphene (%)
Initial	100	100
After 200 cycles	88	77
After 400 cycles	77	74
After 600 cycles	68	69
After 800 cycles	61	69
After 1000 cycles	55	66

Table 3.4. ECSA retention for 20% Pt/XC72 catalyst and Pt/graphene catalyst

	20% Pt/XC72 (%)	Pt/graphene (%)
Initial	100	100
After 200 cycles	39	52
After 400 cycles	12	38
After 600 cycles	10	24
After 800 cycles	9	21
After 1000 cycles	9	20

resistance would lose its binding force with Pt. As a consequence, Pt particles would aggregate to large particles or drop form carbon materials which leads directly to the failure of catalysts. Hence, the carbon corrosion process during ADT cycling was also measured by the integration of the double layer charging (CV curve between 0.4 V to 0.6 V). It is assumed that the carbon corrosion will cause the loss of carbon particles from catalyst layer which may decrease the surface and double layer charging of carbon support. As can be seen from Fig. 3.11, a trend of double layer charging decreasing could be observed with the increasing of ADT cycles. For Pt/graphene catalyst, only little DLC decreases could be observed with the increasing ADT cycle number at the average rate of 0.007 uC/cm^2/100 cycle while Pt/XC72 slope decrease with ADT cycles at the average rate of 0.026 uC/cm^2/100 cycle. This also confirmed our previous discussion that graphene is a better Pt support for the PEMFCs catalysts.

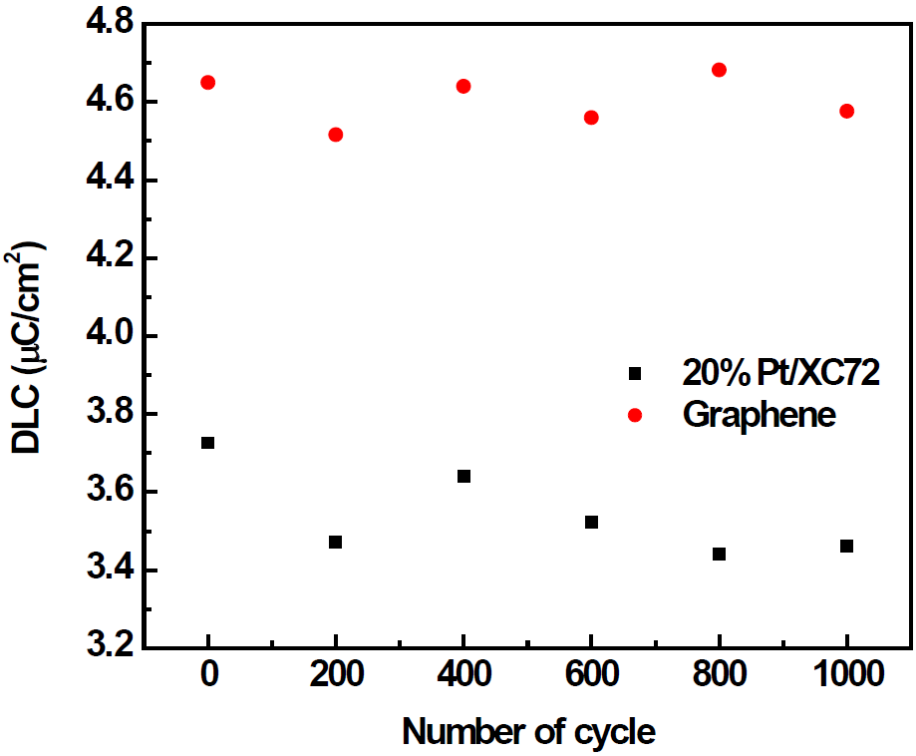

Figure 3.11. Double layer charging (DLC) for 20% Pt/XC72 and Pt/graphene catalyst during ADT

3.3 Conclusion

A simple and effective approach was developed for the preparation of graphene supported Pt nanoparticle catalyst. The Pt nanoparticles with an average size of 2.6 nm were observed uniformly dispersed on the surface of the graphene sheets. The results of ADTs showed that the Pt/graphene catalyst had a better stability than 20% Pt/XC72, although the CV and ORR results demonstrated that the Pt/graphene catalyst exhibited lower electrochemical surface area and oxygen reduction activity in acidic media as compared with 20% Pt/XC72, which was due to the restacking of graphene nanosheet. By comparing the double layer charge difference during ADT process between Pt/graphene catalyst and 20% Pt/XC72, we further confirmed that the loss of electrochemical properties was due to the carbon corrosion and graphene had a better corrosion resistance than XC72 as a catalyst support. Despite the lower ECSA and mass activity which can be further enhanced by introducing spacers to prevent the agglomeration of graphene nanosheets, Pt/graphene catalyst synthesized by synchronous reduction method developed a highly durable graphene-based catalyst for PEMFCs applications. However, restacking is still a major problem for Pt/graphene catalyst that hinders its application into fuel cell to replace Pt/XC72 catalyst.

4. PT/FG/FCG CATALYST FOR PEMFC APPLICATION

4.1 Experimental

4.1.1 Experiment Material and Instrument

Materials

All materials used are listed in Table 4.1.

Table 4.1. Materials

Chemical name	Purity	Provider
Chloroplatinic acid ($H_2PtCl_6xH_2O$)	99.9%	Acros Organics
Carbon black Vulcan XC-72	Not specified	Cabot, MA
Nafion solution	5wt%	Ion Power Inc.
Graphite powder	99.8%	Alfa Aesar
Ethylene glycol	99.8%	Sigma-Aldrich
Sodium borohydride ($NaBH_4$)	99%	Acros Organics
Ammonium hudroxide	28-30wt%	Fisher Scientific
70% perchloric acid solution	99.999%	Fisher Scientific
Isopropanol alcohol (IPA)	99.9%	Fisher Scientific
High purity de-ionized (DI) water	18MΩ	Millipore
20% Pt/XC72 catalyst (E-TEK)	Not specified	BASF
Sulfanilic acid	98wt%	Alfa Aesar
P-phenylenediamine	97wt%	Alfa Aesar
Hydrochloric acid (HCl)	36.5-36.8wt%	Fisher Scientific
Sulfuric acid (H_2SO_4)	95-98wt%	Fisher Scientific
Sodium Nitrate ($NaNO_2$)	98wt%	Alfa Aesar
Hydrogen (H_2)	5.0 UHP	Praxair
Oxygen (O_2)	5.0 UHP	Praxair

All chemicals were used as received.

Instruments

All instruments used are listed in Table 4.2.

Table 4.2. Instruments

Instrument	Provider
Electrochemical workstation	Bio-Logic, TN, USA
Ag/AgCl reference electrode	Pine instruments, PA, USA
Electrode rotator	Pine instruments, PA, USA
Rotating disk electrode (RDE)	Pine instruments, PA, USA
X-Ray diffractometer	Siemens
Thermogravimetric analyzer (TGA)	TA instrument
Transmission electron microscopy	From Argonne National Lab
Gas sorption analyzer	Quantachrome Instruments, FL, USA
Freeze drier	Labconco, MO, USA
Vacuum oven	VWR
Centrifuge	Thermo scientific
Ultrasonic bath	Branson, CT, USA

4.1.2 Experiment Methods

Synthesis of Functional Carbon Black with -SO_3H Functional group

Functionalized carbon black (FCB) was synthesized by diazonium reactions. Carbon black was dispersed in DI water and then was mixed with sulfanilic acid and concentrated HCl under constant stirring for 30 min. Then $NaNO_2$ solution with calculated concentration was added dropwise into the above carbon black dispersion followed by heating to 60°C for 1h. After the reaction was completed, the dispersion was filtered with 500 kilo Dolton membrane and washed by DI water until the collected solution was transparent. Then the remaining solid was dried in a vacuum oven.

Functionalized graphene (FG) was also prepared by similar method. Graphene was dispersed into DI water under sonication. Then phenylenediamine and HCl were added into the dispersion and the solution was sonicated for 30 min.

Synthesis of Pt/graphene Catalyst and Pt/FG/FCB Catalyst

FG/FCB mixture (1:1 in weight ratio) was dispersed into the ethylene glycol aqueous solution (EG: H_2O = 3:2) followed by sonicating for 1 h and stirring overnight. Calculated amount of $H_2PtCl_6 \cdot 6H_2O$ solution (10 mg/ml) was then added into the above dispersion and was stirred for 1 h. The dispersion was then refluxed at 140 °C for 6 h. Then remaining solid was collected by filtration and washed by water and then freeze dried in freeze drier.

4.1.3 Characterization

The morphology, particle size of the Pt/FG/FCB catalyst powder was examined using transmission electron microscopy (TEM). Thermogravimetric analysis (TGA) was carried out to determine the Pt loading on the carbon support. Brunauer, Emmett and Teller method was applied to measure the specific surface area and pore size distribution of the Pt/FG/FCB catalyst was measured using a gas sorption analyzer.

4.1.4 Electrochemical Performance

The electrochemical performance of Pt/FG/FCB was measured under the same condition as Pt/graphene catalyst to ensure the consistence of experiment.

4.2 Result and Discussion

4.2.1 Characterization of Pt/FG/FCB Catalyst

The TGA result of FG and FCB are shown in Fig. 4.1. It can be seen that similar trend could be observed for FG and FCB compared to that of pure GO. There are also two weight loss processes corresponding to the thermo decomposition of functional groups in FG/FCB and graphene in the catalyst. This indicates that the functional group is successfully grafted on the surface of graphene and carbon black.

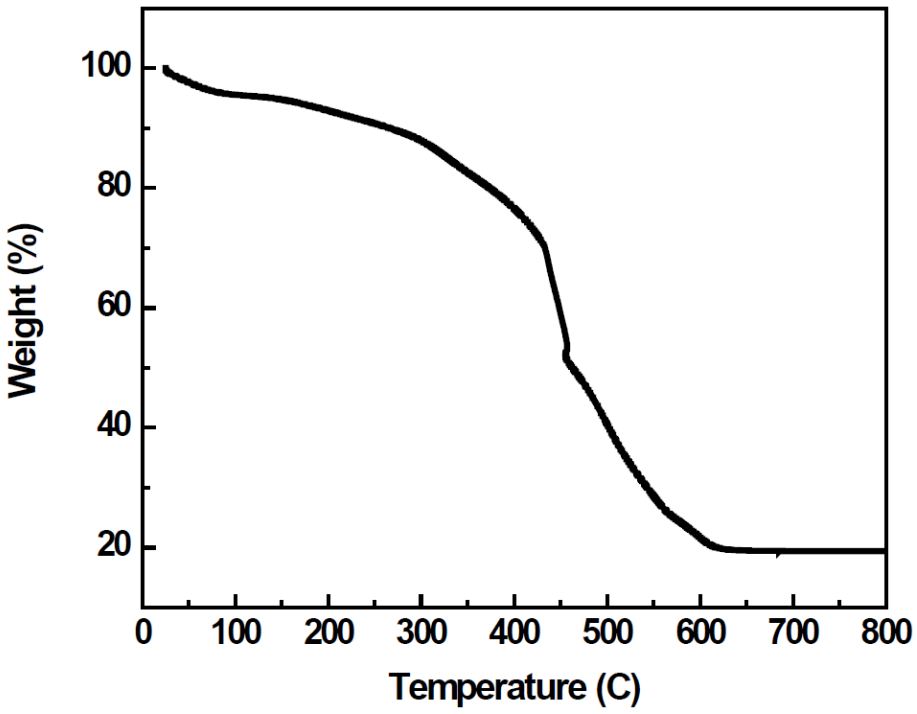

Figure 4.1. TGA curves of Pt/FG/FCB

The TEM picture of Pt/FG/FCB is shown in Fig. 4.2. From the picture, it can be seen that Pt nano particles are uniformly distributed on the graphene surface and FCB particles are successfully inserted between graphene sheets as spacers. The average Pt particle size according to TEM picture is 2.17 nm. The spacers are successfully inserted between graphene because of the charge effect. NH_2 function group carries

positive charge in aqueous solution while -COOH function group carries negative charge. The strong charge force bond the FG and FCB together strongly.

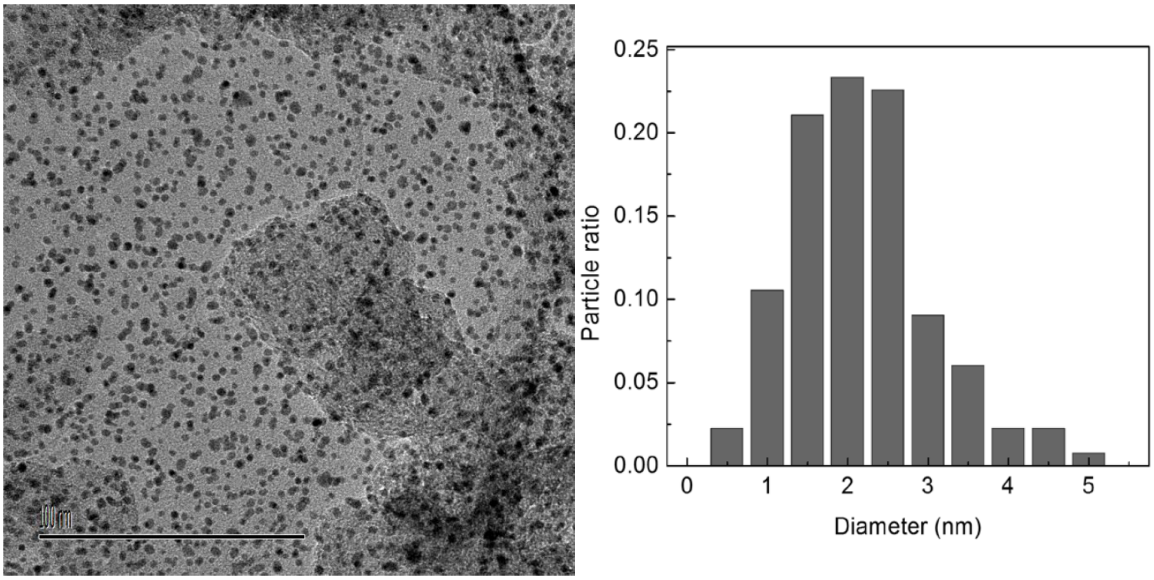

Figure 4.2. (a) TEM picture of Pt/FG/FCB catalyst and size distribution of Pt; (b) Size distribution of Pt particle on FG/FCB catalyst support

The BET method was also applied to test the pore size distribution and average surface area of Pt/FG/FCB catalyst by N_2 gas sorption analyzer. The average specific surface area of the Pt/FG/FCB increases to 96 cm^2/g because of the introducing of FCB spacers. The pore size distribution is shown in Fig. 4.3. As can be seen in the Fig. 4.3, the pore size increases. Some major pores ranged from 10-20 nm can be observed which facilitate the diffusion of electrolyte between graphene layers and be in contact with Pt nanoparticles which improves the performance of the catalyst. All those larger pores are due to the successfully insertion of the FCB spacers which prevent the restacking of the graphene nanosheets.

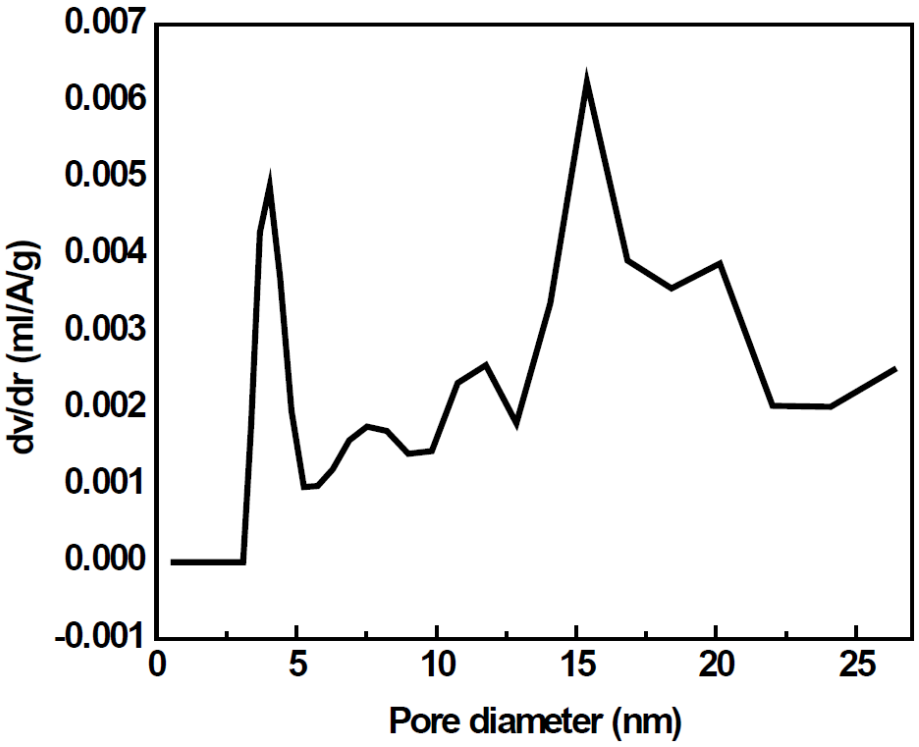

Figure 4.3. Pore size distribution of Pt/FCB/FG catalyst

4.2.2 Electrochemical Performance of Pt/FCB/FG Catalyst

The result of the CV The result of the CV and ORR test of the Pt/FCB/FG catalyst at room temperature were shown in Fig. 4.3. As can be calculated from Fig. 4.4a, the ECSA of Pt/FG/FCB is 40.43 m^2/g Pt which is higher than that of Pt/graphene (35.12 m^2/g Pt) catalyst but lower than that of 20%Pt/XC72 catalyst (65.05 m^2/g Pt). The ECSA of Pt/FG/FCB increases due to the successfully insertion of FCB spacers. The graphene nanosheets are separated by FCB spacers which formed bigger pores as diffusion channel for electrolyte. This is also confirmed by the BET and size distribution result. With more larger pores, more Pt nanoparticles can be exposed to the electrolyte and contribute to the performance. Fig. 4.4b shows the polarization cure of Pt/FCB/FG. The limiting current of Pt/FCB/FG is 5.0 mA/cm^2 which is slightly higher than that of Pt/graphene catalyst. The increment of both ECSA and limiting current mean that the restacking problem is much improved.

The half-wave potential for Pt/FCB/FC catalyst is 0.85 V which is the same as 20% Pt/XC72 catalyst and higher than that of Pt/graphene catalyst. This result indicates that Pt/FCB/FG catalyst has a higher catalytic activity. At 0.9 V, the mass activity of Pt/FCB/FG catalyst is 112 mA/mg Pt which is much higher than that of Pt/graphene catalyst (32 mA/mg Pt) and 20% Pt/XC72 catalyst(76 mA/mg Pt). From the improvement of the mass activity of the catalyst after introducing FCB spacers, we can say that the bond generated by the electrostatic force is strong enough to bond the FCB spacers between graphene and separate the sheet from restacking.

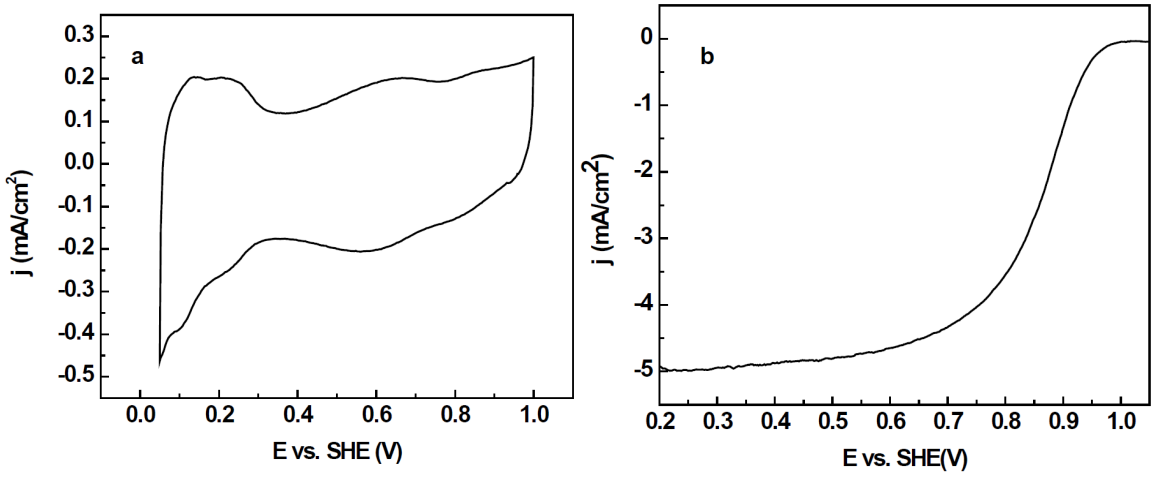

Figure 4.4. (a) CV of Pt/FCB/FG catalyst; (b) Polarization curve of Pt/FCB/FG

ECSA and mass activity data for three different kinds of catalysts are shown in table 4.3. We can find that the mass activity of Pt/FCB/FG is higher than that of 20% Pt/XC72. However, the low ECSA indicates that there is still some restacking and there will be more works to solve this problem to further improve the electrochemical performance of graphene supported Pt catalysts for PEMFCs.

To further investigate the stability of the Pt/FCB/FG catalyst during cycling, ADT test was also applied under the same experiment condition as Pt/graphene catalyst. The ADT result of Pt/FCB/FG is shown in Fig. 4.5. Minor ECSA loss was observed during ADT for Pt/FCB/FG catalyst which indicated that such catalyst was

Table 4.3. Electrochemical data for three kinds of catalysts

	ECSA (m^2/g Pt)	Mass activity (mA/mg Pt)	Half-wave potential (V)
20% Pt/XC72	65	76	0.80
Pt/graphene	35	32	0.75
Pt/FCB/FG	40.43	112	0.80

quite stable. From the polarization curve in Fig. 4.5, we can see that the mass activity at 0.9 V is 23 mAh/mg which is much smaller than that of Pt/XC72 catalyst. At the meantime, the half-wave potential shifts only 0.02 V after ADT. All those ADT data indicates that Pt/FG/FCG catalyst is better than Pt/XC72 catalyst and Pt/XC72 catalyst and Pt/graphene catalyst.

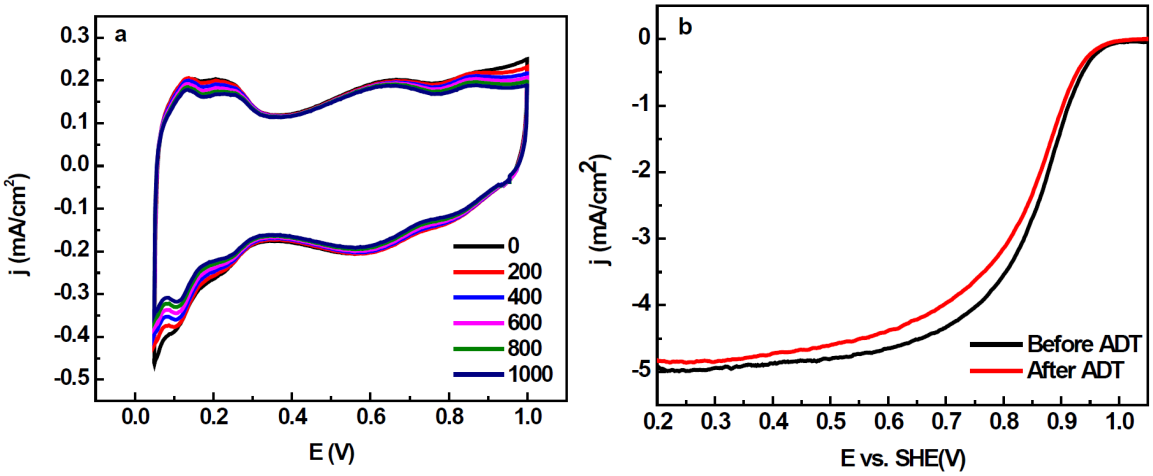

Figure 4.5. CV curve for Pt/FCB/FG during ADT; (b) Polarization curve for Pt/FCB/FG before and after ADT

The ECSA retention is also plotted into Fig. 4.6. It can be seen that Pt/FCB/FG catalyst performed much better than Pt/XC72 catalyst. The decay rate for Pt/FCB/FG catalyst is 1.5%/100 cycles which is slower than that of Pt/XC72 catalyst (4.5%/100 cycles). This result also indicates that Pt/FCB/FG catalyst is much better than Pt/XC72 catalyst and Pt/graphene catalyst.

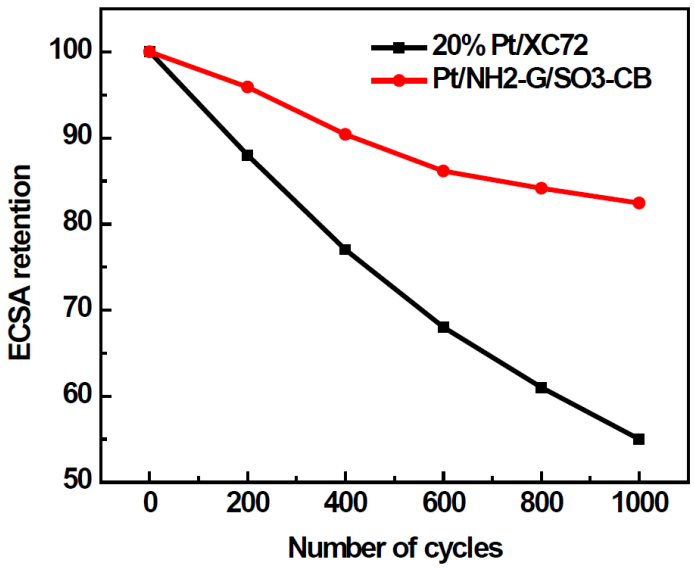

Figure 4.6. ECSA retention for three kinds of catalysts

4.3 Conclusion

FCB particles were introduced into Pt/graphene catalyst as spaces to prevent the restacking of graphene nanosheets. The electrostatic force will anchor FCB onto the surface of graphene nanosheets to ensure the successful introducing of spacers. TEM pictures proved that the spacers were inserted between graphene nanosheets successfully. FCB particles in the catalyst were used to prevent the restacking of graphene nanosheets and with the help of spacers, the electrochemical performance of Pt increased significantly which was higher than that of 20% Pt/XC72 catalyst. The durability of Pt/FCB/FG catalyst is much better than that of 20% Pt/XC72 catalyst because of the highly graphitic structure. With higher mass activity and much higher durability, Pt/FCB/FG catalyst is a more promising catalyst than 20% Pt/XC72 catalyst that could be commercialized and applied in PEMFCs.

5. SUMMARY

In this work, a simple synchronous synthesis method was used to prepare Pt/graphene catalyst. According to electrochemical test results, it has lower ECSA and mass activity but higher durability than 20% Pt/XC72 catalyst. The low ECSA and mass activity was due to the restacking of graphene nano sheet which blocked the pathway for diffusion. The high durability was due to the highly graphitic structure of graphene which has higher resistance to corrosion during cycling.

To improve the catalytic performance and solve the restacking problem of Pt/ graphene catalyst, graphene was functionalized and FCB which carried opposite charges was introduced as spacers to prevent the restacking of graphene nanosheets. TEM image showed that the spacers were inserted between graphene nanosheets successfully. Pt/FCB/FG catalyst also showed a higher mass activity than 20% Pt/XC72 catalyst. However, the lower ECSA indicated the restacking still existed. Further work needs to be done to solve the restacking problem to further increase the mass activity of such catalyst.

Generally speaking, with much higher durability and higher mass activity, Pt/FCB/ FG catalyst will replace 20% Pt/XC72 catalyst in the market of PEMFC catalysts in the future.

REFERENCES

REFERENCES

[1] H. A. Gasteiger, S. S. Kocha, B. Sompalli, and F. T. Wagner, "Activity benchmarks and requirements for pt, pt-alloy, and non-pt oxygen reduction catalysts for pemfcs," *Applied Catalysis B: Environmental*, vol. 56, no. 1, pp. 9–35, 2005.

[2] Z. Z. Le Xin, Z. Wang, J. Qi, and W. Li, "Carbon supported ag nanoparticles as high performance cathode catalyst for h2/o2 anion exchange membrane fuel cell," *Frontiers in Chemistry*, vol. 1, 2013.

[3] K. Mayrhofer, D. Strmcnik, B. B. Blizanac, V. Stamenkovic, M. Arenz, and N. M. Markovic, "Measurement of oxygen reduction activities via the rotating disc electrode method: From pt model surfaces to carbon-supported high surface area catalysts," *Electrochimica Acta*, vol. 53, no. 7, pp. 3181–3188, 2008.

[4] D. Strmcnik, K. Kodama, D. Van der Vliet, J. Greeley, V. R. Stamenkovic, and N. M. Marković, "The role of non-covalent interactions in electrocatalytic fuel-cell reactions on platinum," *Nature Chemistry*, vol. 1, no. 6, pp. 466–472, 2009.

[5] N. Marković and P. N. Ross, "Surface science studies of model fuel cell electrocatalysts," *Surface Science Reports*, vol. 45, no. 4, pp. 117–229, 2002.

[6] Z. Zheng, H. Fang, F. Yang, Z.-K. Liu, and Y. Wang, "Amorphous lilatio3 as solid electrolyte material," *Journal of The Electrochemical Society*, vol. 161, no. 4, pp. A473–A479, 2014.

[7] C. Jia, Q. Liu, C.-J. Sun, F. Yang, Y. Ren, S. M. Heald, Y. Liu, Z.-F. Li, W. Lu, and J. Xie, "In situ x-ray near-edge absorption spectroscopy investigation of the state of charge of all-vanadium redox flow batteries," *ACS Applied Materials & Interfaces*, vol. 6, no. 20, pp. 17 920–17 925, 2014.

[8] Y. Cui and Y. Fu, "Polysulfide transport through separators measured by a linear voltage sweep method," *Journal of Power Sources*, vol. 286, pp. 557–560, 2015.

[9] Q. Liu, Z.-F. Li, Y. Liu, H. Zhang, Y. Ren, C.-J. Sun, W. Lu, Y. Zhou, L. Stanciu, E. A. Stach *et al.*, "Graphene-modified nanostructured vanadium pentoxide hybrids with extraordinary electrochemical performance for li-ion batteries," *Nature Communications*, vol. 6, 2015.

[10] R. C. Alkire and C. W. Tobias, *Advances in Electrochemical Science and Engineering*. John Wiley & Sons, 2008, vol. 5.

[11] R. L. Borup, J. R. Davey, F. H. Garzon, D. L. Wood, and M. A. Inbody, "Pem fuel cell electrocatalyst durability measurements," *Journal of Power Sources*, vol. 163, no. 1, pp. 76–81, 2006.

[12] J. Xie, D. L. Wood, D. M. Wayne, T. A. Zawodzinski, P. Atanassov, and R. L. Borup, "Durability of pefcs at high humidity conditions," *Journal of The Electrochemical Society*, vol. 152, no. 1, pp. A104–A113, 2005.

[13] P. Ferreira, Y. Shao-Horn, D. Morgan, R. Makharia, S. Kocha, H. Gasteiger *et al.*, "Instability of pt/ c electrocatalysts in proton exchange membrane fuel cells a mechanistic investigation," *Journal of The Electrochemical Society*, vol. 152, no. 11, pp. A2256–A2271, 2005.

[14] K. Yasuda, A. Taniguchi, T. Akita, T. Ioroi, and Z. Siroma, "Platinum dissolution and deposition in the polymer electrolyte membrane of a pem fuel cell as studied by potential cycling," *Physical Chemistry Chemical Physics*, vol. 8, no. 6, pp. 746–752, 2006.

[15] H. Gasteiger, J. Panels, and S. Yan, "Dependence of pem fuel cell performance on catalyst loading," *Journal of Power Sources*, vol. 127, no. 1, pp. 162–171, 2004.

[16] F. De Bruijn, V. Dam, and G. Janssen, "Review: durability and degradation issues of pem fuel cell components," *Fuel Cells*, vol. 8, no. 1, p. 3, 2008.

[17] K. G. Gallagher, D. T. Wong, and T. F. Fuller, "The effect of transient potential exposure on the electrochemical oxidation of carbon black in low-temperature fuel cells," *Journal of The Electrochemical Society*, vol. 155, no. 5, pp. B488–B493, 2008.

[18] J. G. de la Fuente, S. Rojas, M. Martínez-Huerta, P. Terreros, M. Pena, and J. Fierro, "Functionalization of carbon support and its influence on the electrocatalytic behaviour of pt/c in h 2 and co electrooxidation," *Carbon*, vol. 44, no. 10, pp. 1919–1929, 2006.

[19] H. Tang, M. Pan, F. Wang, P. K. Shen, and S. P. Jiang, "Highly durable proton exchange membranes for low temperature fuel cells," *The Journal of Physical Chemistry B*, vol. 111, no. 30, pp. 8684–8690, 2007.

[20] A. C. Fernandes and E. A. Ticianelli, "A performance and degradation study of nafion 212 membrane for proton exchange membrane fuel cells," *Journal of Power Sources*, vol. 193, no. 2, pp. 547–554, 2009.

[21] A. Guha, W. Lu, T. A. Zawodzinski, and D. A. Schiraldi, "Surface-modified carbons as platinum catalyst support for pem fuel cells," *Carbon*, vol. 45, no. 7, pp. 1506–1517, 2007.

[22] D. Stevens and J. Dahn, "Thermal degradation of the support in carbon-supported platinum electrocatalysts for pem fuel cells," *Carbon*, vol. 43, no. 1, pp. 179–188, 2005.

[23] F. Xu, M.-x. Wang, Q. Liu, H.-f. Sun, S. Simonson, N. Ogbeifun, E. A. Stach, and J. Xie, "Investigation of the carbon corrosion process for polymer electrolyte fuel cells using a rotating disk electrode technique," *Journal of the Electrochemical Society*, vol. 157, no. 8, pp. B1138–B1145, 2010.

[24] T. K. Lee, J. H. Jung, J. B. Kim, and S. H. Hur, "Improved durability of pt/cnt catalysts by the low temperature self-catalyzed reduction for the pem fuel cells," *International Journal of Hydrogen Energy*, vol. 37, no. 23, pp. 17 992–18 000, 2012.

[25] M. Kim, J.-N. Park, H. Kim, S. Song, and W.-H. Lee, "The preparation of pt/c catalysts using various carbon materials for the cathode of pemfc," *Journal of Power Sources*, vol. 163, no. 1, pp. 93–97, 2006.

[26] A. L. Dicks, "The role of carbon in fuel cells," *Journal of Power Sources*, vol. 156, no. 2, pp. 128–141, 2006.

[27] F. von Sturm, "Carbon materials. carbonelectrochemical and physicochemical properties. by k. kinoshita. wiley, new york 1988. xiii, 533 pp., bound,£ 65.00.isbn 0-471-84802-6," *Angewandte Chemie*, vol. 100, no. 9, pp. 1260–1261, 1988.

[28] K. H. Kangasniemi, D. Condit, and T. Jarvi, "Characterization of vulcan electrochemically oxidized under simulated pem fuel cell conditions," *Journal of The Electrochemical Society*, vol. 151, no. 4, pp. E125–E132, 2004.

[29] F. Xu, M.-x. Wang, L. Sun, Q. Liu, H.-f. Sun, E. A. Stach, and J. Xie, "Enhanced pt/c catalyst stability using p-benzensulfonic acid functionalized carbon blacks as catalyst supports," *Electrochimica Acta*, vol. 94, pp. 172–181, 2013.

[30] T. Matsumoto, T. Komatsu, K. Arai, T. Yamazaki, M. Kijima, H. Shimizu, Y. Takasawa, and J. Nakamura, "Reduction of pt usage in fuel cell electrocatalysts with carbon nanotube electrodes," *Chemical Communications*, no. 7, pp. 840–841, 2004.

[31] M.-x. Wang, F. Xu, Q. Liu, H.-f. Sun, R.-h. Cheng, H. He, E. A. Stach, and J. Xie, "Enhancing the catalytic performance of pt/c catalysts using steam-etched carbon blacks as a catalyst support," *Carbon*, vol. 49, no. 1, pp. 256–265, 2011.

[32] M.-x. Wang, Q. Liu, H.-f. Sun, N. Ogbeifun, F. Xu, E. A. Stach, and J. Xie, "Investigation of carbon corrosion in polymer electrolyte fuel cells using steam etching," *Materials Chemistry and Physics*, vol. 123, no. 2, pp. 761–766, 2010.

[33] P. Ferreira-Aparicio, M. Folgado, and L. Daza, "High surface area graphite as alternative support for proton exchange membrane fuel cell catalysts," *Journal of Power Sources*, vol. 192, no. 1, pp. 57–62, 2009.

[34] D. Strmcnik, N. Hodnik, S. Hocevar, D. Van der Vliet, M. Zorko, V. Stamenkovic, B. Pihlar, and N. Markovic, "Novel method for fast characterization of high-surface-area electrocatalytic materials using a carbon fiber microelectrode," *The Journal of Physical Chemistry C*, vol. 114, no. 6, pp. 2640–2644, 2010.

[35] S. Yang, G.-L. Zhao, and E. Khosravi, "First principles studies of nitrogen doped carbon nanotubes for dioxygen reduction," *The Journal of Physical Chemistry C*, vol. 114, no. 8, pp. 3371–3375, 2010.

[36] P. V. Shanahan, L. Xu, C. Liang, M. Waje, S. Dai, and Y. Yan, "Graphitic mesoporous carbon as a durable fuel cell catalyst support," *Journal of Power Sources*, vol. 185, no. 1, pp. 423–427, 2008.

[37] M.-x. Wang, F. Xu, H.-f. Sun, Q. Liu, K. Artyushkova, E. A. Stach, and J. Xie, "Nanoscale graphite-supported pt catalysts for oxygen reduction reactions in fuel cells," *Electrochimica Acta*, vol. 56, no. 5, pp. 2566–2573, 2011.

[38] C. Xu, X. Wang, and J. Zhu, "Graphene- metal particle nanocomposites," *The Journal of Physical Chemistry C*, vol. 112, no. 50, pp. 19 841–19 845, 2008.

[39] Y. Shao, G. Yin, Y. Gao, and P. Shi, "Durability study of pt/ c and pt/ cnts catalysts under simulated pem fuel cell conditions," *Journal of the Electrochemical Society*, vol. 153, no. 6, pp. A1093–A1097, 2006.

[40] B. Seger and P. V. Kamat, "Electrocatalytically active graphene-platinum nanocomposites. role of 2-d carbon support in pem fuel cells," *The Journal of Physical Chemistry C*, vol. 113, no. 19, pp. 7990–7995, 2009.

[41] Z.-F. Li, L. Xin, F. Yang, Y. Liu, Y. Liu, H. Zhang, L. Stanciu, and J. Xie, "Hierarchical polybenzimidazole-grafted graphene hybrids as supports for pt nanoparticle catalysts with excellent pemfc performance," *Nano Energy*, vol. 16, pp. 281–292, 2015.

[42] Z.-F. Li, H. Zhang, F. Yang, L. Stanciu, and J. Xie, "Pt catalysts supported on polybenzimidazole-grafted graphene for pemfcs," *ECS Transactions*, vol. 64, no. 3, pp. 131–136, 2014.

[43] A. K. Geim and K. S. Novoselov, "The rise of graphene," *Nature Materials*, vol. 6, no. 3, pp. 183–191, 2007.

[44] M. Lei, C. Liang, Y. Wang, K. Huang, C. Ye, G. Liu, W. Wang, S. Jin, R. Zhang, D. Fan *et al.*, "Durable platinum/graphene catalysts assisted with polydiallyldimethylammonium for proton-exchange membrane fuel cells," *Electrochimica Acta*, vol. 113, pp. 366–372, 2013.

[45] Y. Li, Y. Li, E. Zhu, T. McLouth, C.-Y. Chiu, X. Huang, and Y. Huang, "Stabilization of high-performance oxygen reduction reaction pt electrocatalyst supported on reduced graphene oxide/carbon black composite," *Journal of the American Chemical Society*, vol. 134, no. 30, pp. 12 326–12 329, 2012.

[46] S. Guo, S. Dong, and E. Wang, "Three-dimensional pt-on-pd bimetallic nanodendrites supported on graphene nanosheet: facile synthesis and used as an advanced nanoelectrocatalyst for methanol oxidation," *ACS Nano*, vol. 4, no. 1, pp. 547–555, 2009.

[47] Y. Si and E. T. Samulski, "Exfoliated graphene separated by platinum nanoparticles," *Chemistry of Materials*, vol. 20, no. 21, pp. 6792–6797, 2008.

[48] Z.-F. Li, H. Zhang, Q. Liu, Y. Liu, L. Stanciu, and J. Xie, "Covalently-grafted polyaniline on graphene oxide sheets for high performance electrochemical supercapacitors," *Carbon*, vol. 71, pp. 257–267, 2014.

[49] M.-x. Wang, Q. Liu, H.-f. Sun, E. A. Stach, H. Zhang, L. Stanciu, and J. Xie, "Preparation of high-surface-area carbon nanoparticle/graphene composites," *Carbon*, vol. 50, no. 10, pp. 3845–3853, 2012.

[50] S. Liu, J. Wang, J. Zeng, J. Ou, Z. Li, X. Liu, and S. Yang, "green electrochemical synthesis of pt/graphene sheet nanocomposite film and its electrocatalytic property," *Journal of Power Sources*, vol. 195, no. 15, pp. 4628–4633, 2010.

[51] R. Shah, "Introduction to fuel cells," in *Recent Trends in Fuel Cell Science and Technology*. Springer, 2007, pp. 1–9.

[52] S. Litster and G. McLean, "Pem fuel cell electrodes," *Journal of Power Sources*, vol. 130, no. 1, pp. 61–76, 2004.

[53] J. Chen, T. Matsuura, and M. Hori, "Novel gas diffusion layer with water management function for pemfc," *Journal of Power Sources*, vol. 131, no. 1, pp. 155–161, 2004.

[54] K. A. Mauritz and R. B. Moore, "State of understanding of nafion," *Chemical Reviews*, vol. 104, no. 10, pp. 4535–4586, 2004.

[55] K.-D. Kreuer, T. Dippel, W. Meyer, and J. Maier, "Nafion® membranes: Molecular diffusion, proton conductivity and proton conduction mechanism," in *MRS Proceedings*, vol. 293. Cambridge Univ Press, 1992, p. 273.

[56] H. P. Kumar and M. A. Xavior, "Graphene reinforced metal matrix composite (grmmc): A review," *Procedia Engineering*, vol. 97, pp. 1033–1040, 2014.

[57] W. S. Hummers Jr. and R. E. Offeman, "Preparation of graphitic oxide," *Journal of the American Chemical Society*, vol. 80, no. 6, pp. 1339–1339, 1958.

[58] N. I. Kovtyukhova, P. J. Ollivier, B. R. Martin, T. E. Mallouk, S. A. Chizhik, E. V. Buzaneva, and A. D. Gorchinskiy, "Layer-by-layer assembly of ultrathin composite films from micron-sized graphite oxide sheets and polycations," *Chemistry of Materials*, vol. 11, no. 3, pp. 771–778, 1999.

[59] W. Gao, L. B. Alemany, L. Ci, and P. M. Ajayan, "New insights into the structure and reduction of graphite oxide," *Nature Chemistry*, vol. 1, no. 5, pp. 403–408, 2009.

[60] Z.-F. Li, H. Zhang, Q. Liu, L. Sun, L. Stanciu, and J. Xie, "Fabrication of high-surface-area graphene/polyaniline nanocomposites and their application in supercapacitors," *ACS Applied Materials & Interfaces*, vol. 5, no. 7, pp. 2685–2691, 2013.

[61] E. W. Washburn, "The dynamics of capillary flow," *Physical Review*, vol. 17, no. 3, p. 273, 1921.

[62] H.-W. Chang, Y.-C. Tsai, C.-W. Cheng, C.-Y. Lin, and P.-H. Wu, "Preparation of graphene-supported platinum nanoparticles in aqueous solution by femtosecond laser pulses for methanol oxidation," *Journal of Power Sources*, vol. 239, pp. 164–168, 2013.

[63] Q.-L. Zhang, T.-Q. Xu, J. Wei, J.-R. Chen, A.-J. Wang, and J.-J. Feng, "Facile synthesis of uniform pt nanoparticles on polydopamine-reduced graphene oxide and their electrochemical sensing," *Electrochimica Acta*, vol. 112, pp. 127–132, 2013.

[64] Y. Liu, Y. Xia, H. Yang, Y. Zhang, M. Zhao, and G. Pan, "Facile preparation of high-quality pt/reduced graphene oxide nanoscrolls for methanol oxidation," *Nanotechnology*, vol. 24, no. 23, p. 235401, 2013.

[65] A. Pozio, M. De Francesco, A. Cemmi, F. Cardellini, and L. Giorgi, "Comparison of high surface pt/c catalysts by cyclic voltammetry," *Journal of Power Sources*, vol. 105, no. 1, pp. 13–19, 2002.